DE-AC02-76ER01198

DOE/ER/01198/1390

LOW-TEMPERATURE THERMAL EXPANSION OF AMORPHOUS SOLIDS

BY

DAVID ALAN ACKERMAN

B.A., Cornell University, 1976
M.S., University of Illinois, 1978

THESIS

Submitted in partial fulfillment of the requirements
for the degree of Doctor of Philosophy in Physics
in the Graduate College of the
University of Illinois at Urbana-Champaign, 1982

Urbana, Illinois

PACS indices: 61.40.-a
65.70.+y
63.50.+x
07.20.-n

DISCLAIMER

DOE/ER/01198--1390

DE83 001128

LOW-TEMPERATURE THERMAL EXPANSION OF AMORPHOUS SOLIDS

BY

DAVID ALAN ACKERMAN

B.A., Cornell University, 1976
M.S., University of Illinois, 1978

THESIS

Submitted in partial fulfillment of the requirements
for the degree of Doctor of Philosophy in Physics
in the Graduate College of the
University of Illinois at Urbana-Champaign, 1982

Urbana, Illinois

PACS indices: 61.40.-a
65.70.+y
63.50.+x
07.20.-n

THIS PAGE

WAS INTENTIONALLY

LEFT BLANK

LOW-TEMPERATURE THERMAL EXPANSION OF AMORPHOUS SOLIDS

David Alan Ackerman, Ph.D.
Department of Physics
University of Illinois at Urbana-Champaign, 1982

For most amorphous materials at temperatures below $\approx$ 1 K, the magnitudes and temperature dependences of specific heat, thermal conductivity and ultrasonic dispersion are qualitatively similar, independent of chemical composition. It has been suggested that thermal expansion also exhibits this universal behavior. The development of a dilatometer capable of resolving sample strains as small as 10^{-12} has permitted measurement of the linear thermal expansion of various glasses below 1 K. These investigations have demonstrated, however, that the low-temperature thermal expansion coefficient of glasses can be positive, negative, large or small. Analysis of measurements performed on two types of vitreous silica, two amorphous polymers, As_2S_3 and $ZrO_2 : Y_2O_3$ is presented in the context of the phenomenological tunneling-states model. Consistency in explanation of thermal expansion and ultrasonic behavior is maintained by assuming a broad, weakly energy-dependent distribution of coupling strengths between phonons and the localized excitations thought to be characteristic of the glassy state.

ACKNOWLEDGMENTS

The author would like to thank his advisor, Prof. A. C. Anderson for inspiration, invaluable guidance and infinite patience.

Thanks also go to Terry Smith and Dean Matsumoto for providing the SiO_2 and SC5 samples, J. J. Fontenella for supplying the As_2S_3 sample and Mike MacDonald and Fred Walker for sharing their specific heat data on SiO_2 and $ZrO_2 : Y_2O_3$.

Thanks to fellow workers for assistance in the lab and to friends, in particular, Terry, Dean, Brian and Steve, for sharing a lot of beer at Murphy's.

The author very gratefully thanks his parents and brother, Wayne, for constant understanding and moral support. Finally, a special thanks must go to Ada Tymiak, for love, companionship and support over the last seven years.

This work was supported in part by the National Science Foundation, under Grant DMR80-06941 and the Materials Sciences Division of the Department of Energy, under Grant DE-AC02-76ER01198. The author acknowledges the support of a fellowship provided by the General Electric Foundation.

TABLE OF CONTENTS

Page

I. INTRODUCTION

Low temperature properties of amorphous materials have been the subject of experimental and theoretical investigation for over a decade.[1] In the course of this time, a large body of evidence has been gathered from which two fundamental observations can be made: (i) Below 1 K, thermal and acoustic properties of most amorphous dielectrics are qualitatively similar in magnitude and temperature dependence (Fig. 1);[2-15] (ii) This characteristic signature of the glassy state is markedly different from that of pure dielectrics in the crystalline state (Fig. 2).[2,16-19]

The first observation (i) seems to reflect the influence of some feature intrinsic to the glassy state, but independent of chemical composition or structure. The second observation (ii) implies that this feature, universal to glasses, is absent in crystals. It is puzzling to note that on the length scale of $\gtrsim$ 1000 Å set by 1 K thermal phonons, both crystals and glasses should be well approximated by elastic continua. As such, low temperature thermal and acoustic properties should be similar for both groups of materials, not reflecting structural differences on the scale of short range order or disorder. Experimental evidence to the contrary, showing that glasses behave universally as a group and anomalously relative to crystals, has set the stage for a problem which, as yet, remains fundamentally unsolved.

Theories of glasses at low temperatures have taken various forms.[20-28] However, one phenomenological model has emerged which best fits experimental observations to date.[20,21,25] In its present form, this theory proposes the existence of a broad energy band of localized

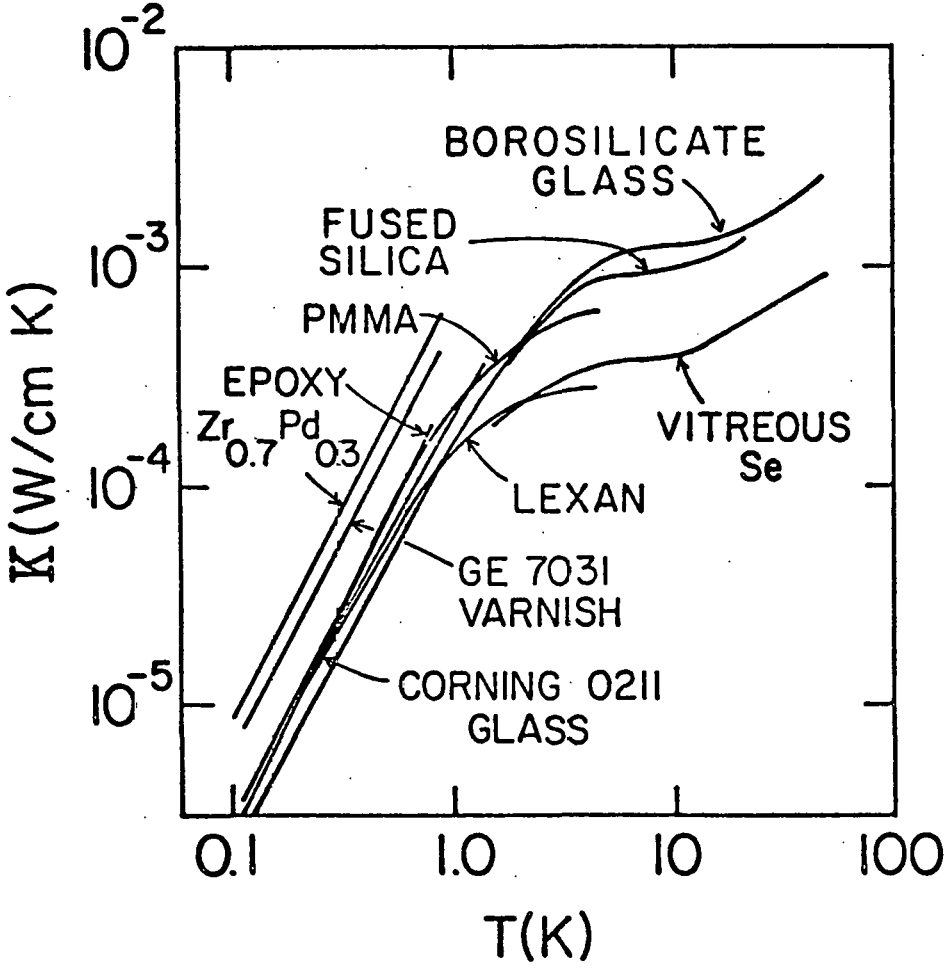

Figure 1. Thermal conductivities of assorted amorphous materials. Fused silica (Ref. 2), Borosilicate glass (Ref. 3), Corning 0211 glass (Ref. 4), PMMA (Ref. 5), Epoxy (Ref. 6), Lexan (Ref. 7), GE 7031 varnish (Ref. 8), Vitreous selenium (Ref. 9), Superconducting $Zr_{0.7}Pd_{0.3}$ (Ref. 10).

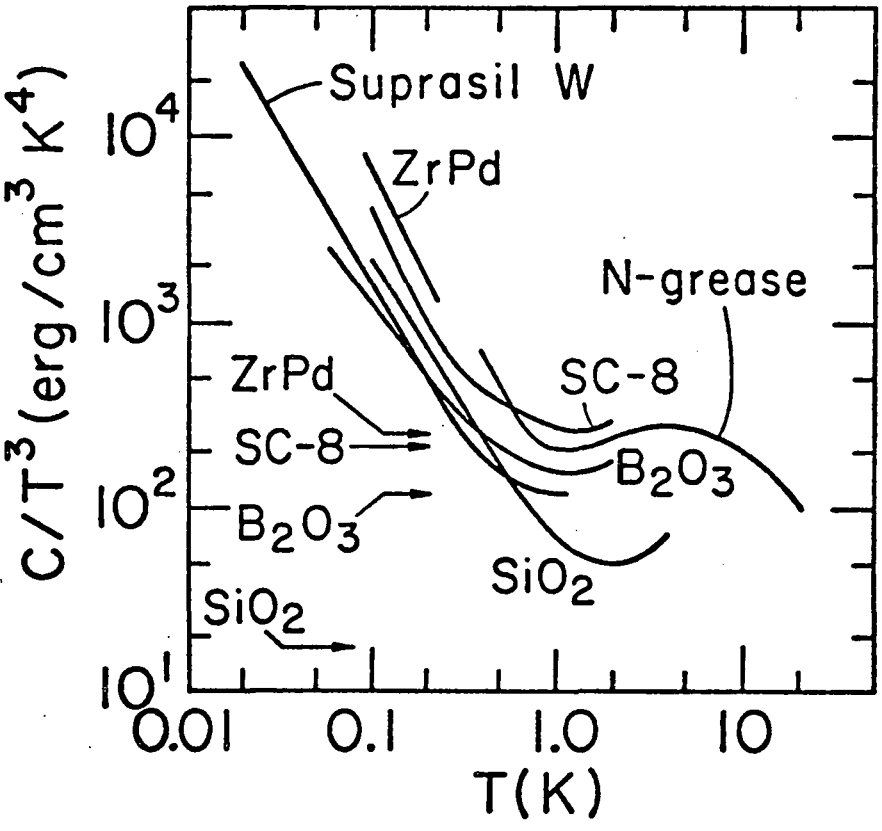

Specific heat divided by T^3 for assorted amorphous materials. $Zr_{0.7}Pd_{0.3}$ (Ref. 10), SC8 epoxy (Ref. 11), Apiezon N grease (Ref. 12), B_2O_3 (Ref. 13), Suprasil W (Ref. 14), Spectrosil B (Ref. 15). Arrows indicate magnitudes of Debye phonon contribution to specific heat.

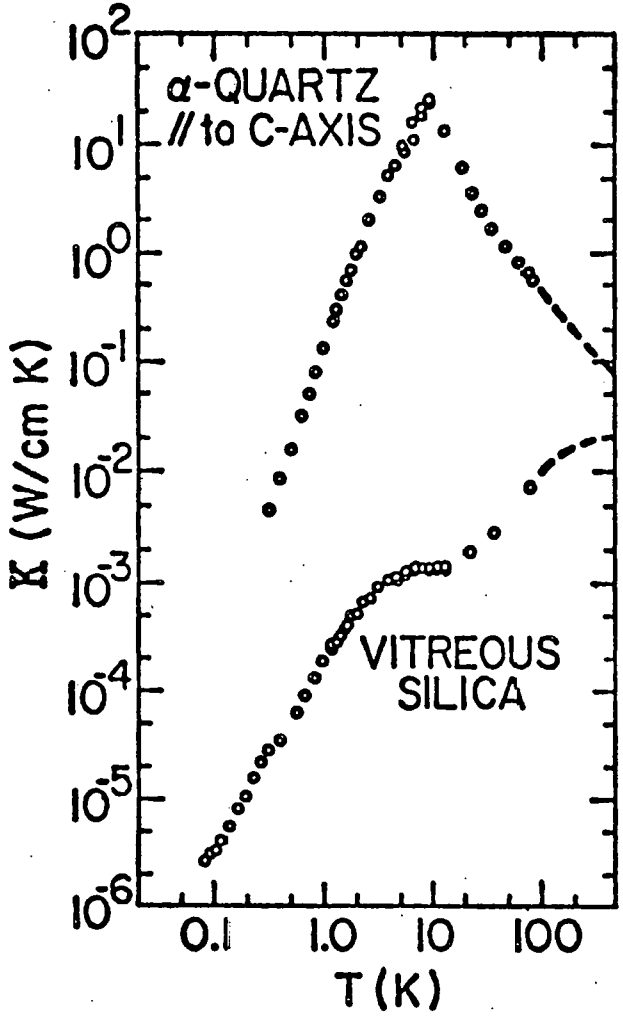

Figure 2. Comparison of the measured thermal conductivity of an α-quartz crystal to that of fused silica, showing the effect of long range order (Ref. 2).

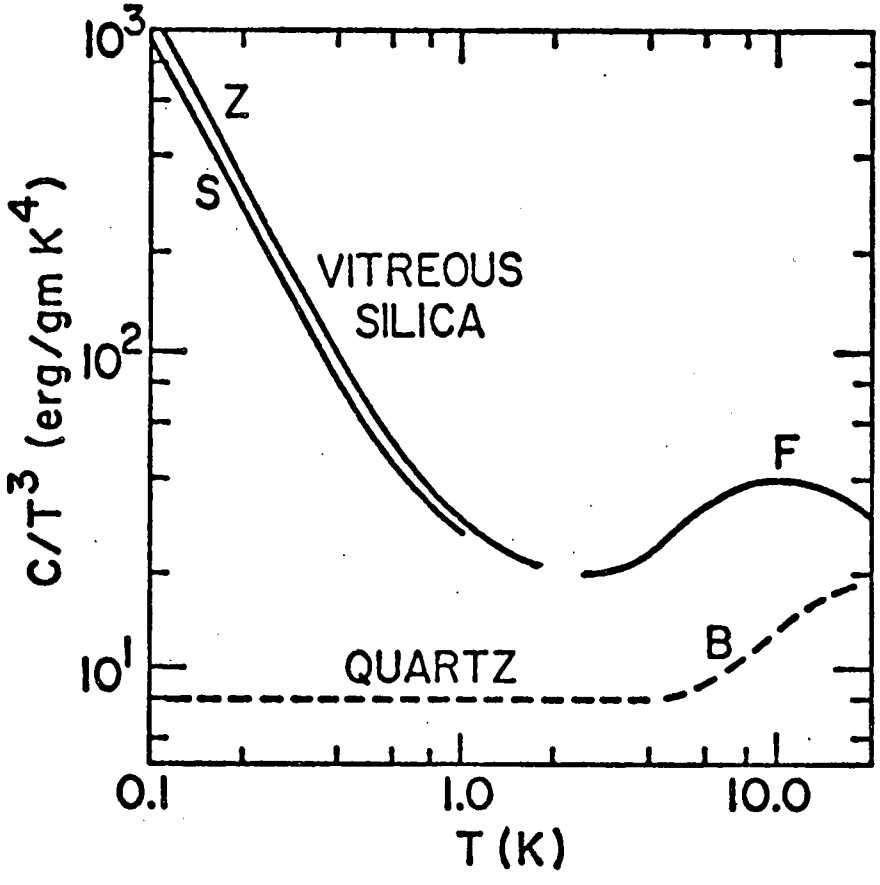

Comparison of the measured specific heat, divided by T^3, of α-quartz to that of fused silica. Z (Ref. 16), S (Ref. 17), F (Ref. 18), B (Ref. 19).

excitations which couple strongly to phonons. These excitations are characterized as having a ground state and one excited state well separated from states of higher energy, hence the name two-level-state (TLS). Tunneling of some entity or configuration between potential energy minima, separated by a large barrier, is cited as a possible origin of these TLS.[20-21] However, in no amorphous material, whether through tunneling or by a different mechanism, is the microscopic origin of the TLS understood.

The presence of a broad energy spectrum occurring universally in glasses has prevented extraction of detailed material-specific information. Thus, the understanding of amorphous materials at low temperatures has, in recent years, remained stalled at a phenomenological level. Efforts to probe effects of disorder below 1 K have turned to materials with structure which may be more easily defined than that of glass, e.g., crystals with 2-dimensional disorder,[29] radiation damaged crystals,[30] doped crystals[31] and plastic crystals.[32] The goal in these investigations has been the precise association of low temperature properties with better characterized structural disorder. While this approach is probably impossible in amorphous materials, a suggestion has been made that thermal expansion below 1 K could provide new information relating thermal properties to structure.[33] This test may probe the sensitivity of TLS to local environment, and hence provide unique information on material-dependent properties--an attractive prospect. In practice, however, the measurement necessitates detection of sample strains as small as 10^{-12}.[34]

Thermal expansion is the variation of physical dimension of a material with temperature. A linear thermal expansion coefficient $\alpha(T)$ is defined as $\alpha(T) \equiv (\partial \ell nL / \partial T)_p$, from which a volumetric coefficient $\beta(T)$ can be written as $\beta(T) = \sum_i \alpha_i (T)$, $i = x,y,z$. For isotropic materials, $\beta = 3\alpha$, as might be expected for amorphous materials. While the Debye or continuum model is sufficient for understanding such properties as specific heat of pure crystalline dielectrics, it is inadequate in accounting for thermal expansion. In the Debye approximation, normal mode (phonon) frequencies are assumed to be independent of both volume and temperature, rendering $\beta(T) \equiv 0$. By introducing volume (and temperature) dependent frequencies,[35] thermal expansion can be included, at the expense of an additional layer of theoretical complexity. Dependence of frequency ω on volume, i.e., anharmonicity, reflects coupling of phonon modes to external strain and consequently, coupling of phonon modes to one another. In a simple approximation, $-\partial \ell n\omega_i / \partial \ell nV \equiv \Gamma_i$, constant for mode i, giving rise to the Grüneisen equation of state,[36] $\beta B = \Gamma C$. (C = specific heat, B = bulk modulus, $\Gamma = \sum_i \Gamma_i C_i / \sum_i C_i$, C_i = heat capacity of i-th mode.) Γ, a measure of anharmonicity, can then be related to the experimentally measured quantities, B, $\beta(T)$ and $C(T)$.

In the case of amorphous materials, the question of thermal expansion shifts focus from phonon-phonon coupling (important at higher temperatures) to coupling between phonons and TLS.[37] Such coupling is measured in ultrasonic attenuation experiments[38] and allows a prediction of thermal expansion to be made. This estimate must be based on a physical picture of the excitation and as such, comparison of measured and

predicted values comprises a test of any particular model of excitation (as discussed in Chapter V). Specifically, measurement of $\beta(T)$ should reflect the presence of tunneling entities postulated to be the source of the low-lying excitations.[39] Indeed, large values of Γ (outside of the "normal" range of 1-3) occur in doped alkali halide crystals in which tunneling of impurities is documented.[40] A question arises as to whether the TLS will contribute to a thermal expansion signature in amorphous solids which is universal to glasses, and anomalous relative to crystals.

The aim of this study was to try to gain new insight into low-temperature glassy behavior through the measurement of thermal expansion of various amorphous materials. In particular, the connection between observed acoustic properties of localized excitations and thermal expansion was explored.

In the course of this work, a new dilatometric technique was developed[41] which made possible, for the first time, thermal expansion measurements of pure glasses below 1 K. Utilizing a SQUID in a position-sensitive detector circuit, this dilatometer proved capable of detecting length changes of $\lesssim 10^{-3}$ Å with a resolution of 2×10^{-4} Å. This represents a 100 fold increase in sensitivity over conventional techniques. The absolute accuracy of the data is believed to be ± 10%. Preliminary measurements of $\alpha(T)$ of high purity copper were performed demonstrating satisfactory performance of the dilatometer.

Thermal expansion measurements proceeded on an assortment of amorphous dielectrics having widely varying chemical composition and

and structure. In brief, it was discovered that $\alpha(T)$ for glasses could be positive, negative, large or small. This result was in contrast to a suggestion[27,42,59] that thermal expansion, in analogy to other thermal properties of glasses, should be universal in character. Results indicated, for the first time, the influence of material-dependent parameters upon glassy behavior.

Chapter II contains a review of previous experimental and theoretical efforts directed toward understanding thermal expansion of glasses. In Chapter III is a description of the SQUID dilatometer while Chapter IV contains experimental results of measurements on amorphous materials obtained using this apparatus. Chapter V provides a discussion of these results followed by a brief conclusion.

II. PREVIOUS WORK

Introduction

Thermal and acoustic properties of many glasses have been studied over a wide range in temperature extending down to ~0.01 K.[1,43] For the purpose of this review, these investigations can be grouped roughly into two categories, those directed toward properties of glasses above ~4 K and those specifically designed to observe universal glassy behavior below helium temperature. The former group, discussed in the next section, consists largely of investigations of vitreous silica (amorphous SiO_2), in part for its utility as a low expansivity construction material and reference standard. Anomalous thermal and elastic properties of silica, as well as other amorphous materials, were linked to chemical composition, structure, thermal history and other material-dependent parameters.[17,44-49]

With the extension of studies to below 1 K, glassy properties were found to be remarkably independent of those sample-dependent parameters mentioned above,[16] and instead, related simply to the presence of disorder. The resulting low-temperature experimental activity in the field of amorphous materials was followed by several phenomenological models of the glassy state.[20-28] A brief review of the most successful (to date) of these theories will follow later in this chapter. Until the present however, thermal expansion measurements have been restricted to $T > 1.5$ K; a result of the difficulty of detecting small length changes occurring at very low temperatures. The last section of this chapter contains a review of those low-temperature thermal expansion experiments designed to test, at $T > 1.5$ K, the intrinsic properties of the glassy state.

Studies Above ~4 K

That vitreous silica exhibits negative thermal expansion down to at least 10 K was known by 1959.[44] This effect in silica was unexplained however, as were a large low-temperature ultrasonic absorption, positive pressure and negative temperature coefficients of elastic moduli, and a specific heat in excess of that predicted from acoustic data.[45] In contrast, B_2O_3 glass, while having a similar excess specific heat,[17] exhibited positive low-temperature expansion.[46] It was further discovered that the magnitude of the thermal expansion coefficient $\beta(T)$ of vitreous silica could be reduced, and the sign changed to positive, by addition of network-filling impurities.[47] These bits of evidence led to the conjecture that low-frequency vibrational modes, considered to be responsible for enhanced specific heat, might also contribute to thermal expansion in certain glasses.[48] The existence of transverse modes, with negative Grüneisen parameters, was hypothesized as the origin of negative expansivity and was associated with the "open" structure of tetrahedrally bonded glasses.[49] Justification for this reasoning came by analogy to diamond structure solids such as silicon, germanium, gallium arsenide and diamond, for which negative thermal expansion is observed at $T \lesssim 100$ K.[49,50] Significantly however, the magnitude of the negative expansion coefficients for these crystalline materials reaches a maximum at $T \approx \theta_D / 15$. At lower temperatures, thermal behavior conforms to that predicted by elastic theory.[49] In contrast, negative thermal expansion was observed in vitreous silica at temperatures as low as $\theta_D / 200$.[33]

In addition to the idea of low frequency vibrations as explanation for anomalous thermal properties of glasses, suggestions of a discrete set of either Einstein modes[18] or excitations giving rise to Schottky peaks[51] were offered. While these theories addressed unexplained properties of glasses, each was designed around a particular material or subgroup of solids. Nevertheless, the work outlined above formed the foundation from which lower temperature thermal expansion studies of glasses were extended.

Studies Below 4 K

Below 1 K, amorphous materials differ in thermal and acoustic properties from crystalline materials of the same chemical composition. For example, specific heat of crystals may be represented as $C(T) = C_D T^3$. C_D, given by Debye theory, is dependent on ultrasonic velocities in a given crystal.[52] For a wide variety of glasses however, $C(T) \approx C_1 T^1 + C_3 T^3$ in which $C_1 \sim 30$ erg/K^{2}cm^3 and $C_3 \approx$ (1.2 to 3) x C_D.[17] Thermal conductivity of crystals at low temperatures may be written as $\kappa(T) = (C_D T^3)\ \bar{v}\ell/3$;[52] $\bar{v}$ is an average sound velocity, ℓ is an appropriate sample dimension. In contrast, thermal conductivity of, once again, a wide variety of glasses can be represented as $\kappa(T) = \kappa_o (T/1K)^{\delta}$, $\kappa_o \approx 10^{-4}$ W/cm K, $\delta \approx 1.9 \pm 0.1$.[17] Thus, glasses exhibit enhanced specific heat and drastically reduced thermal conductivity relative to pure crystals.

The suggestion of a connection between these phenomena was first advanced in 1971.[16] A set of excitations which could store energy and scatter phonons was proposed as a general feature of the amorphous state,

accounting for the observed properties. That these excitations were localized and that Debye phonons served as thermal carriers was established experimentally.[53] Through ultrasonic work it was determined that at low temperatures each excitation had a limited number of accessible states (for example, a ground state and one excited state) and that coupling between phonons and localized excitations was very strong.[54] Specific heat measurements revealed that the distribution in energy of the excitations was broad. The proposal of a broad energy-independent spectrum of localized excitations (modelled as two-level-states) as the basis of low-temperature glassy behavior has proven to be most useful in interpreting experimental results. As a model, it is phenomenological in nature however, making no precise statement about excitations in any particular amorphous material. The generality of the problem renders this an advantage on one hand, but a shortcoming when questions of chemical composition or morphology are posed. As has been mentioned, thermal expansion is related to the volume dependence of energy levels in a system. The two-level-states (TLS) model makes no a priori assumptions about this type of dependence, leaving predictions of low-temperature thermal expansion in an indefinite state. Implied however, is that information relating TLS excitation energy to volume could serve to augment the model and perhaps sharpen the focus on localized excitations in particular materials. This question will be examined in Chapter V.

Existence of a broad band of two-level-state excitations in glasses has been explained as arising through quantum mechanical tunneling. The tunneling-states model hypothesizes that certain entities

within a disordered solid might reside in a potential with two (or more) local equilibrium positions, separated by barriers (Fig. 3). Under conditions which would effectively prohibit barrier hopping--low temperatures and small but finite overlap between potential wells--tunneling between equilibrium positions could become significant. Tunneling would serve to couple the otherwise independent ground state wave-functions of the system creating, for example, a pair of states well separated from states of higher energy. Such a two-level-state would represent a localized excitation which, through strain modulation of its physical dimensions or its local environment,[38] could couple to Debye phonons. The lack of order, characteristic of a glass, could provide a variety of such tunneling sites resulting in the observed broad distribution of splitting energies. Alternatively,[55] a single characteristic TLS energy might be broadened through random TLS-TLS interaction yielding the same energy-independent density of states. Thus, the model accounts for the necessary features of the proposed excitations. It should be noted that any model capable of providing these features would be acceptable. A more detailed discussion of the TLS model is contained in the next section.

The Tunneling-States Model

Rigorous treatment of the tunneling-states model can be found elsewhere[20,21,25,56]--a condensed version will be presented below. The first step is representation of the localized excitation as a mass m in a one-dimensional potential pictured in Fig. 3. Using as basis states, the ground state wavefunctions of the individual wells (which are not

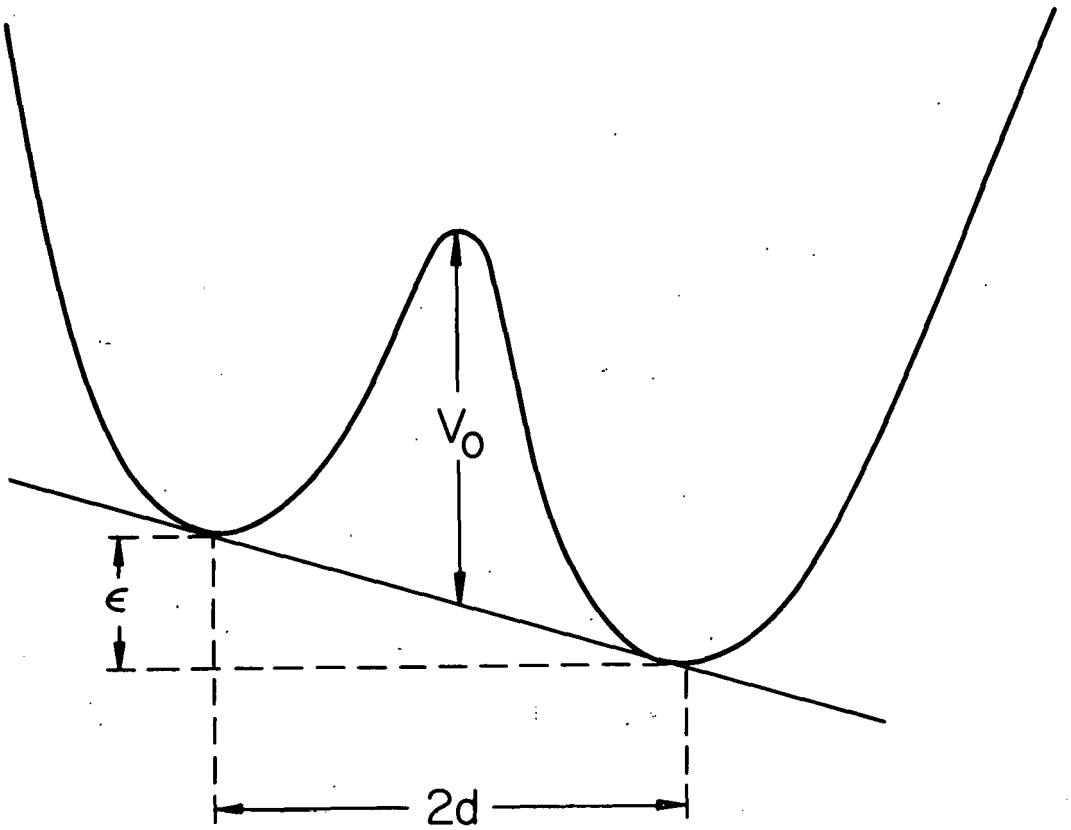

Figure 3. A schematic representation of a tunneling state. Potential energy is plotted vertically versus spatial ccordinate. Each individual well is a harmonic oscillator potential. V_o is the barrier height, ϵ is the asymmetry and 2d is the well separation.

eigenstates of the total potential), a Hamiltonian H_o^* can be constructed[38] (* indicates representation in single well basis).

$$H_o^* = \begin{pmatrix} \varepsilon & \Delta \\ \Delta & -\varepsilon \end{pmatrix} \qquad \text{II-1}$$

in which

ε = asymmetry energy

$$\Delta = \text{overlap energy} = \hbar\omega_o e^{-\lambda} \text{[20,21]} \qquad \text{II-2}$$

$$\lambda = \left(\frac{V_o}{\hbar^2 / 2md^2} \right)$$

Perturbation of the potential by a strain wave of amplitude e gives rise to a first order correction H_1^*.[38]

$$H_1^* = \sum_{\alpha\beta} \left(\frac{\partial}{\partial e_{\alpha\beta}} H_o^* \right) e_{\alpha\beta} \qquad \text{II-3}$$

in which

$e_{\alpha\beta}$ = local strain tensor.

For simplicity, the tensor notation will be suppressed at this point. In practice, a scalar approximation is sufficient in many calculations.

The next step is to change basis states to eigenstates of the double well potential. Upon rotation,

$$H_o^* \rightarrow H_o = \frac{1}{2}\begin{bmatrix} E & 0 \\ 0 & -E \end{bmatrix} \qquad \text{II-4}$$

$$E = (\varepsilon^2 + \Delta^2)^{1/2}$$

and

$$H_1^* \rightarrow H_1 = \frac{1}{2}\begin{bmatrix} D & 2M \\ 2M & D \end{bmatrix} e \qquad \text{II-5}$$

in which

$$D = \frac{\varepsilon}{E}\frac{\partial \varepsilon}{\partial e} + \frac{\Delta}{E}\frac{\partial \Delta}{\partial e} \qquad \text{II-6}$$

and

$$2M = -\frac{\varepsilon}{E}\frac{\partial \Delta}{\partial e} + \frac{\Delta}{E}\frac{\partial \varepsilon}{\partial e} \qquad \text{II-7}$$

are tensor deformation potentials.[38] D is a measure of the variation of splitting energy with strain while M gives the strength of coupling between ground and excited states due to strain.[38]

The distribution in energy of TLS is assumed to be broad, essentially constant over the energy range accessible at low temperatures.[20,21] Specifically, it is suggested[21] that the density of states be constant in ε and λ (Eq. II-2), within bounds set by physical constraints. Thermal properties are then computed as averages over these distributions.

It is the coupling to phonons which allows a system of TLS to achieve thermal equilibrium with a host glass. The characteristic time τ_j for the j-th tunneling site to return to equilibrium, once disturbed, is given by[20,21]

$$\tau_j^{-1} = \sum_i \frac{M_j^2}{\rho v_i^2} (2\pi\hbar^4 v_i^3)^{-1} E_j^3 \coth(E_j / 2kT) \qquad \text{(II-8)}$$

in which ρ = mass density of material, v_i = velocity of sound of the i-th phonon mode and E_j, M_j are the splitting energy and resonant coupling strength of the j-th TLS (assuming $\partial\Delta / \partial e \ll \partial\varepsilon / \partial e$[38]). The contribution to heat capacity by this same j-th TLS is

$$C_j = k \left(\frac{E_j}{2kT} \operatorname{sech} \frac{E_j}{2kT} \right)^2 \qquad \text{II-9}$$

In the calculation of total heat capacity of a population of TLS, account must be taken of the experimental time scale t_{exp}, as those TLS with $\tau_i > t_{exp}$ will not respond in time to be measured. This time dependent specific heat is discussed elsewhere.[57] Its effects may be neglected in the present treatment since τ_i, of the TLS in the energy range of interest, is shorter than the τ_{exp}, of $\simeq$ 1 sec. By simply summing over a constant energy density of states n_o,[20,21]

$$C(T) = \frac{\pi^2 k^2 n_o T}{6} \qquad \text{II-10}$$

As mentioned, it has been experimentally established[53] that Debye phonons are responsible for thermal transport in amorphous dielectrics. The magnitude of thermal conductivity is therefore dependent on the mean-free-path of these carriers. In addition to sample dimensions, phonon mean-free-path in glasses is limited by scattering due to TLS, described in terms of two mechanisms.[25,38] The first is a resonant process in which a phonon of frequency ω is absorbed by a TLS of $E = \hbar\omega$ and subsequently reradiated, through spontaneous or stimulated emmission, in a different

direction. Calculation of the resonant scattering rate of a phonon in mode i by the j-th TLS yields a result which is proportional to the square of the resonant matrix element for that particular phonon and TLS, namely $|M_{j,i}|^2$. By assumption, $|M|^2$ is the same for all TLS. The total contribution to scattering by this process is obtained by integration over all TLS, and results in a scattering proportional to $n_o |M|^2 T^{-1}$.[38] Measurement of low temperature specific heat, thermal conductivity and ultrasonic dispersion therefore yield a value for $|M|$.[38]

A second scattering process involving relaxation of TLS is dominant at higher temperatures,[25,38] In this case, a TLS is driven out of thermal equilibrium through modulation of its splitting energy by a phonon strain wave. At a rate determined by its relaxation time (Eq. II-8), the TLS equilibrates by exchanging energy with the phonon bath. Calculation of relaxation scattering due to the j-th TLS predicts a rate proportional to the product $|M_j|^2 |D_j|^2$.[38] After integration over all TLS, a relaxation scattering rate proportional to $n_o \langle M^2 \rangle \langle D^2 \rangle T^3$ is obtained. Comparison to the experimentally observed scattering rate (and knowledge of n_o and $\langle M^2 \rangle$) yields $\langle D^2 \rangle$. Values of ~1eV have been obtained for both $|M|$ and $|D|$ from ultrasonic experiments,[38] under the assumption that M_j and D_j are the same for all TLS.

Evidence supporting the tunneling hypothesis in the form of specific heat, thermal conductivity and ultrasonic measurements has been reviewed.[38,43] Thermal expansion data have proven harder to interpret, in part due to the phenomenological nature of the model and further, due to the paucity of data below 2 K. However, some expansion data have been

taken with the objective of studying the behavior of low-temperature glassy excitations. This material will be discussed next, along with its interpretation.

Thermal Expansion Studies

Measurement of the TLS contribution to thermal expansion has been suggested as a test of the tunneling hypothesis.[33] This proposal is based on observations that, in crystals containing impurities, the expansion coefficient may be very large if the impurity can reorient by tunneling. For example,[40] Grüneisen parameters Γ for KCl containing 100 ppm Li^+ and NaCl containing 80 ppm OH^- are reported to be 300 and 40, respectively. Γ for NaCl containing 130 and 500 ppm CN^- were large and negative.[40] In contrast, Γ for most pure materials falls within the narrow range of 1 to 3. Large Grüneisen parameters have been interpreted in terms of a coupling between phonons and tunneling impurities via modulation of Δ, the overlap energy discussed earlier.[58]

In order to probe localized excitations in glasses, thermal expansion efforts ideally should be directed toward the temperature range below 1.0 K. It is in this regime that the excitations are observed to dominate thermal properties such as specific heat and thermal conductivity, whereas above 1 K, phonon contributions tend to mask TLS effects. However, the technical difficulty of resolving sample strains below 1 K (discussed in Chapter III) has restricted previous investigations of thermal expansion to $T \gtrsim 1.5$ K.[33,42,59,60] Data for three glassy materials, vitreous silica,[33,59,60] PMMA,[59] and As_2S_3[42] have been reported--results and interpretations will be reviewed next.

Thermal expansion of amorphous SiO_2[33] has been measured down to 1.5 K. A distinct low temperature departure from the T^3 dependence of crystals was observed for samples of Spectrosil "1000" and Vitreosil "1400" as well for glassy SiO_2 containing 8% TiO_2.[33] From these data, $\Gamma = -47 \pm 7$ was inferred. In another study of Vitreosil, direct measurement of Γ by an adiabatic compression technique,[60] yielded results in agreement with those of Ref. 33. In the experiment of Ref. 60, oscillating strains of 10^{-5} to 10^{-4} were applied to a sample and consequent changes in temperature were recorded. Γ was deduced through the relationship $\Gamma = -\partial \ell nT / \partial \ell nV \big|_S$. Note that this definition of Γ is thermodynamically identical to that used in Ref. 33, namely $\Gamma = \beta(T)B / C(T)$, and is intrinsically a function of temperature.

A third investigation of amorphous SiO_2 reported somewhat different results, $\Gamma = -16$.[59] Discrepancy between these and the results of Ref. 33 were attributed to experimental technique. The Grüneisen parameter Γ ascribed to the excitations was actually deduced from fits to specific heat, $C(T) = C_1T^1 + C_3T^3$, and thermal expansion, $\beta(T) = \beta_1T^1 + \beta_3T^3$, from which $\Gamma = \beta_1 B_T / C_1$, a constant. This procedure requires the risky extrapolation of $\beta(T)$ and $C(T)$ to $T = 0$ in order to extract linear terms.

It was further discovered that addition of a network filling impurity (Na_2O or CaO) to SiO_2 glass modified thermal expansion behavior above 2 K.[47] With increasing Na_2O concentration, the magnitude of Γ decreased until at 25% Na_2O, the sign of Γ switched from negative to positive at ~10 K. From 25% to 40% concentration, Γ increased in a positive sense.

Thermal expansion data of an amorphous polymer, polymethylmethacrylate (PMMA) have also been taken as low as T = 1.5 K.[59] Using the same fitting procedure described for the silica data, a value of $\Gamma = -16$ was derived. That Γ for both amorphous SiO_2 and PMMA appeared to be the same was taken as a preliminary sign of universal glassy behavior in thermal expansion.[59] However, in the investigation of Ref. 59, all $\beta(T)$ data for PMMA were positive, negative Γ being a result of extrapolation to T = 0.

Finally, an expansion study of arsenic trisulfide was performed.[42] As_2S_3 is a chalcogenide glass which, in contrast to vitreous silica, is known to exhibit positive thermal expansion above 2 K. From data above 1.5 K, using a polynomial fit as in Ref. 59, Γ for As_2S_3 was extrapolated to a T = 0 value of -25.[42] This result was offered as further evidence for an anomalous, negative and universal Γ as characteristic of the glassy state.

Interpretation of thermal expansion data through use of the TLS model is restricted by lack of available microscopic information about localized exictations in any particular glass. Under various assumptions, Γ has been predicted to be potentially very large[27,39,61] or small,[59] universal to glasses[59] or possibly material-dependent.[39] Thermal expansion data at $T \gtrsim 2$ K have been used as evidence both to support[33] and refute[59] the TLS model.

A starting point for discussion of thermal expansion $\beta(T)$ is Eq. II-4 which gives the energy splitting E of a TLS as a function of overlap energy Δ and asymmetry energy ε. In analogy to $\beta(T)$ for

pure crystals, a Grüneisen equation of state[36] can be formulated as $\beta(T)\, B = \Gamma\, C(T)$ in which $\Gamma = \sum_i \Gamma_i C_i / \sum_i C_i$, C_i = heat capacity of i-th TLS, $\Gamma_i = -\partial \ell n E_i / \partial \ell n V$ = Grüneisen parameter of the i-th TLS. Therefore differentiating Eq. II-4,

$$\Gamma_i = -\frac{1}{E}\left(\frac{\varepsilon}{E}\frac{\partial \varepsilon}{\partial e} + \frac{\Delta}{E}\frac{\partial \Delta}{\partial e}\right)_i \qquad \text{II-11}$$

in which

e = local strain tensor.

The strain derivatives or deformation potential tensors appearing above are unknowns which must be included in treating $\beta(T)$ in the TLS model. Absence of microscopic information has left open to argument the relative importance of the two terms on the right hand side of equation II-11. Evidence from ultrasonic experiments has indicated strong coupling of phonons to TLS with deformation potentials ~1eV,[54] but use of this information has varied.

Use of the term $\partial \Delta / \partial e$: Inspection of equation II-2 shows that variation of overlap energy with strain may result from changes in single-well frequency ω, barrier height V_o, or well separation d. Contribution to Γ from $\partial \Delta / \partial e$ has been argued to be small,[38] $\partial \Delta / \partial e$ being of order Δ which, in the energy range of interest, is $\sim 10^{-4}$ eV. Averaging over a density of states, constant in both λ (see Eq. II-2) and ε,[21] estimates of $|\Gamma|$ due solely to variation in overlap range from ~1[39] to ~10.[59] In the latter case, $|\Gamma| \simeq 10$ was derived for a "symmetric tunneling model"

($\varepsilon = 0$ for most TLS)[59] which is at variance with experiment[54] and with the original model in the broad distribution in ε. Approximate verification of this prediction[59] was therefore interpreted as a strike against the TLS model as it is described above. A modified model[42] reconciled results of Ref. 59 and the model of Ref. 20 and 21 by invoking TLS with $E \approx V_o$. With this type of potential however, higher energy states would become accessible--a result not borne out by experiment.[54] In another estimate, reasoning that changes in overlap due to strain might be very large in glasses by analogy to doped alkali halides,[58] values of $|\Gamma| \gtrsim 15$ have been derived.

Use of the term $\partial\varepsilon / \partial e$: There is even less agreement in consideration of variation of asymmetry ε with strain. Arguing that such a deformation potential can originate not only from variation of well parameters, but from "variation in local environment,"[38] it is suggested that changes in asymmetry can provide large $|\Gamma|$. Along different lines but with a similar result, it has been demonstrated that correlation in signs of $\partial\varepsilon / \partial e$ and ε at each TLS can result in $|\Gamma| \approx 10^4$ at 1 K.[39] This hypothesis has been criticized for lack of an a priori basis for such correlations.[62] Similarly, it has been argued that the deformation potential due to asymmetry energy should result in $|\Gamma| \approx 3$ as it derives from "normal lattice interactions."[59] Thus, while all four experiments are suggestive of anomalous $\beta(T)$ for glasses below 1.5 K, interpretation has varied, leaving in question the relationship of TLS and thermal expansion.

In summary of Chapter II, even before the discovery of a low temperature glassy signature, thermal expansion anomalies were seen in amorphous materials at higher temperatures. Below 1 K, glassy properties such as excess heat capacity and small thermal conductivity can be explained using the tunneling-states model. Thermal expansion studies down to 1.5 K show anomalous behavior but do not establish a precise pattern. The current state of theory does not allow a prediction, or even interpretation of these data, to be made unambiguously. All sources cite the need for thermal expansion data at lower temperatures.

III. DILATOMETRY BELOW 1 K

Introduction

This chapter contains a description of the SQUID dilatometer, developed to extend thermal expansion measurements of amorphous materials below 1 K. Construction and operation of the dilatometer are discussed first, followed by test results obtained with high-purity copper.

The difficulty in measuring thermal expansion below 1 K lies in the fact that the expansion coefficient $\alpha(T) = \partial \ell nL / \partial T$ is very small. As an illustration, for copper below 1 K, $\alpha(T) \approx 3 \times 10^{-10}$ T (in units of K^{-1}) and hence, $\delta L = L(3 \times 10^{-10}) T^2 (\delta T / T)$. For a sample of length L = 3 cm, and with $(\delta T / T) \approx 10\%$, $\delta L = (10^{-2} T^2)$ Å. For T = 1 K, δL is already at the limit of resolution reported for conventional capacitive and inductive dilatometric techniques.[35] For measurements to 0.1 K, an improvement in resolution of two orders of magnitude would be needed. It might be possible to achieve the required resolution through improvement of the popular capacitive technique.[35] Instead, a SQUID (Superconducting Quantum Interference Device; detailed description in Ref. 63) was chosen for its high sensitivity as the basis for a displacement sensor.

The SQUID Dilatometer

The operation of the dilatometer may be understood with the help of Fig. 4. The sample S is rigidly restrained at its top end. Appropriate application of power to the electrical heater H causes the

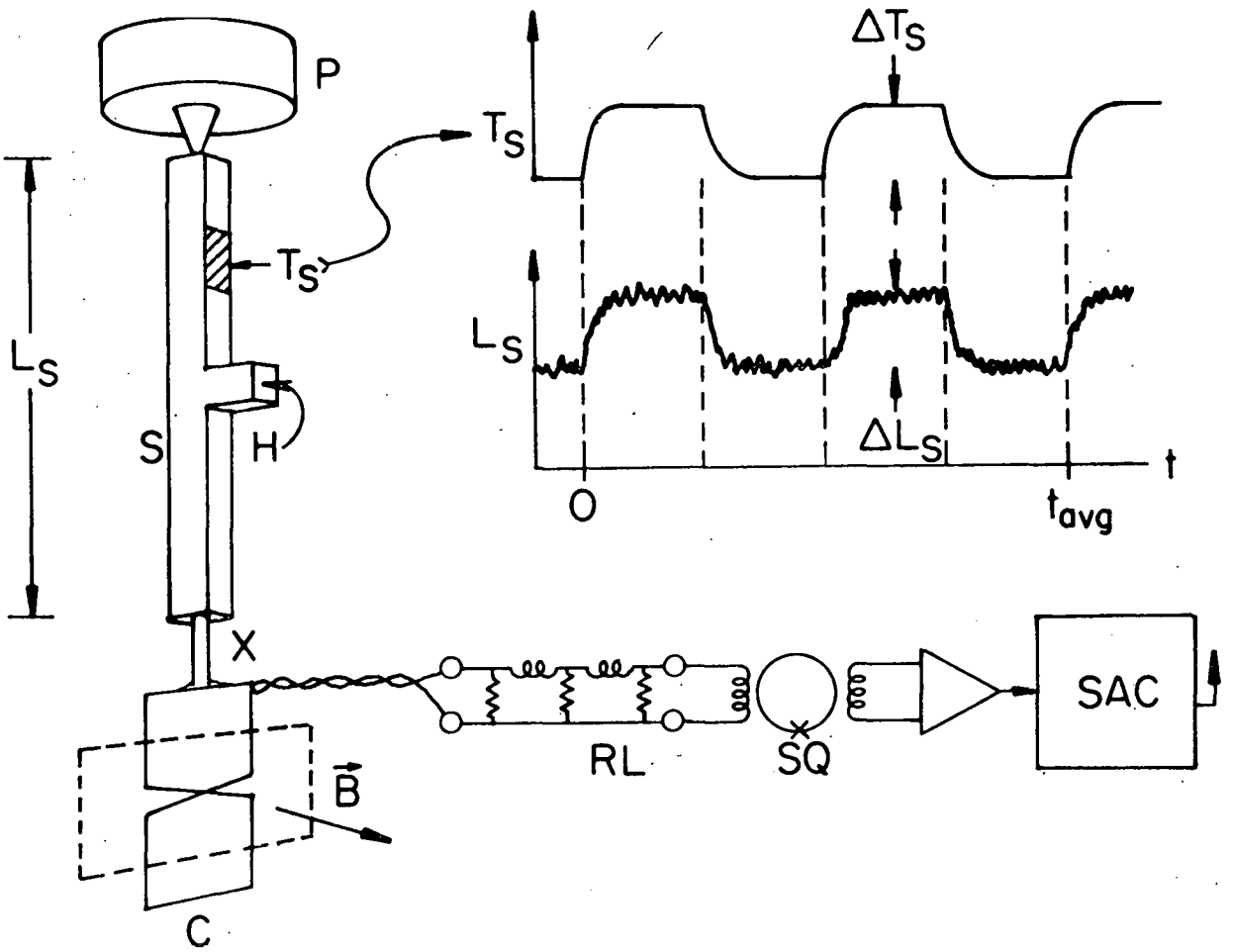

Figure 4. Basic components of the dilatometer. P-piezoelectric transducer; S-sample; T_S-thermometer; H-electrical heater; X-sapphire coupling; C-superconducting coil; $\vec{B}$-field provided by permanent magnet; SQ-SQUID detector; RL-filter; SAC-signal averager. The time variation of the sample temperature T_S, produced by means of heater H, is shown by the upper curve while the output of the SAC, indicating changes in sample length L_S, is shown in the lower curve. The amplitudes of the temperature and length modulations are ΔT_S and ΔL_S, respectively. During each successive time element t_{avg} the SAC averages the output of the SQUID to improve the signal/noise ratio. Typically $\Delta T_S/T_S$ = 10% and t_{avg} = 20 sec.

temperature T_s of the sample to vary periodically with time t as indicated by the T_s - t plot in Fig. 4. In response to the temperature modulation, the length L_s of the sample changes, thereby varying the position of the superconducting coil C relative to a permanent magnetic field $\vec{B}$. The magnetic flux change through the coil, resulting from this change of position, is detected by the SQUID detector SQ. The output of the SQUID is fed to a digital signal-averaging computer SAC which averages successive time periods of duration t_{avg} shown on the L_s - t plot. Signal averaging serves to improve the signal/noise ratio.

The change in length of the sample, ΔL_s, can be obtained from the output signal of the SAC in three ways. First, ΔL_s could be computed from the known dimensions of the superconducting coil, the magnitude of the magnetic field in the gap of the permanent magnet, and the flux sensitivity of the SQUID detector.[64] The accuracy of this computation should be $\approx \pm 30\%$, error originating mainly from estimation of the inductance of coil C. Second, the dilatometer could be calibrated occasionally by measuring a sample of known thermal expansivity. This assumes the dilatometer will retain the calibration between calibration runs, and requires an extrapolation of the calibration to low temperatures since no standards exist for $T < 2$ K. For pure crystalline silicon, considered to be an excellent reference standard, data exist only as low as 6 K.[65]

A third method of calibration places an x-cut quartz piezoelectric transducer within the dilatometer as at P in Fig. 4. The top surface of P is fixed, the lower surface is coupled to the end of the sample.

Application of 44 volts across this transducer causes[66,67] a net length change of ≈ 1.0 Å. However for reasons which were not clear, the apparent output of the transducer varied by as much as 50% between cryogenic runs. After elimination of any electromagnetic pickup between the SQUID and transducer, indications were that the mechanical mounting scheme which coupled the transducer, through the sample, to the detector coil was at fault. Considerable effort to produce an arrangement, reproducible from run to run, met with failure. Other authors have observed this problem.[67] Nevertheless the transducer is useful in conjunction with the second method of calibration discussed above. The transducer output, for a given run, is independent of temperature and is linear in voltage. Hence the transducer may be used to transfer to low temperatures a calibration made against a standard at T > 2 K. Using this technique, the absolute accuracy of the present dilatometer appears to be ≈ ± 10% relative to a standard.

The resolution of the dilatometer is limited by two major problems. The first, vibration transmitted from the environment of the cryostat, would occur for any design. The second, a sensitivity to magnetic fields, is intrinsic to the SQUID system.

The cryostat support had been designed to provide small vibrational amplitudes at the cold-finger of the dilution refrigerator.[68] Examples of precautions taken to minimize vibration include the isolation of mechanical pumps by means of bellows in pumping lines and the isolation of the cryostat frame from the floor using cork cushions and sand. Nevertheless, vibration of the superconducting coil at 5 - 500 Hz

in the 0.4 T field of the permanent magnet induced a changing current which exceeded the maximum slewing rate of the SQUID. The field strength could have been reduced, but not sufficiently to eliminate the problem without sacrificing sensitivity. Instead an RL filter was placed between the superconducting coil and the SQUID as shown in Fig. 4. This filter (see Appendix A) had an attenuation of -10 dB at 1 Hz and rolled off at -60 dB/decade for frequencies greater than 5 Hz. Consistent with this roll-off, the R-L components were selected to minimize Johnson noise and total inductance ($L = 2\mu H$, $R = 3\mu\Omega$). Nevertheless, the resulting Johnson noise, at the output of the SQUID, was equivalent to $\Delta L \lesssim 10^{-2}$ Å. An additional problem introduced by the filter was a large phase shift for frequencies $\gtrsim 1$ Hz. This made it difficult to apply the output of the SQUID to the piezoelectric transducer in a feedback mode to null the motion of the superconducting coil during a measurement. Stable feedback would improve the linearity of the dilatometer by employing the inherently linear response of the transducer. It should be noted however, that a field gradient of $\gtrsim 10^{6}$ T / m would be required to produce a 1% non-linearity in SQUID output as a function of coil position. More typical of the permanent magnet used are gradients $\approx 10^{2}$ T / m. In accordance with this reasoning, it was found (by plotting SQUID output versus voltage to the transducer) that the system was sufficiently linear--feedback was not necessary.

The second problem limiting resolution was the sensitivity of the SQUID circuit to spurious electric and magnetic fields. Fields originating outside the cryostat were reduced by a copper Faraday cage surrounding the cryostat, and by the superconducting lead shield Pb_1 shown

in Fig. 5. Magnetic fields originating within the cryostat were more troublesome. As an illustration, assume the sample to be slightly paramagnetic. The sample resides in the fringing field of the permanent magnet. The imposed temperature variation of Fig. 4 would therefore induce a coherent signal in the superconducting coil (via temperature dependent sample magnetization) which could be interpreted as coil displacement ΔL. Mysterious results obtained in the early stages of development of the dilatometer were traced to such thermo-magnetic effects.

Avoidance of this problem involved enclosing the superconducting coil and the permanent magnet in the superconducting lead shield Pb_2, and maintaining the contents of this shield at a constant temperature while obtaining a datum (see Appendix B). To maintain the constant temperature, the rigid copper frame F of Fig. 5 was thermally isolated from the temperature-regulated refrigerator R by the thermal impedance Z_F. The temperature of the frame was electronically regulated by heater H_F and thermometer T_F. To produce the temperature variation of the sample as shown by Fig. 4, and yet perturb the temperature regulation of the refrigerator as little as possible, a <u>constant</u> power input was switched between heaters H_1 and H_2. The heaters were placed at different distances along a thermal link connecting the sample to the refrigerator and having a finite thermal impedance $Z_1 + Z_2$. The total thermal impedance of the link was chosen to (1) minimize the power needed to raise the sample temperature T_s above that of the refrigerator, and (2) minimize the equilibration time τ_{ext} of the sample, where τ_{ext} =

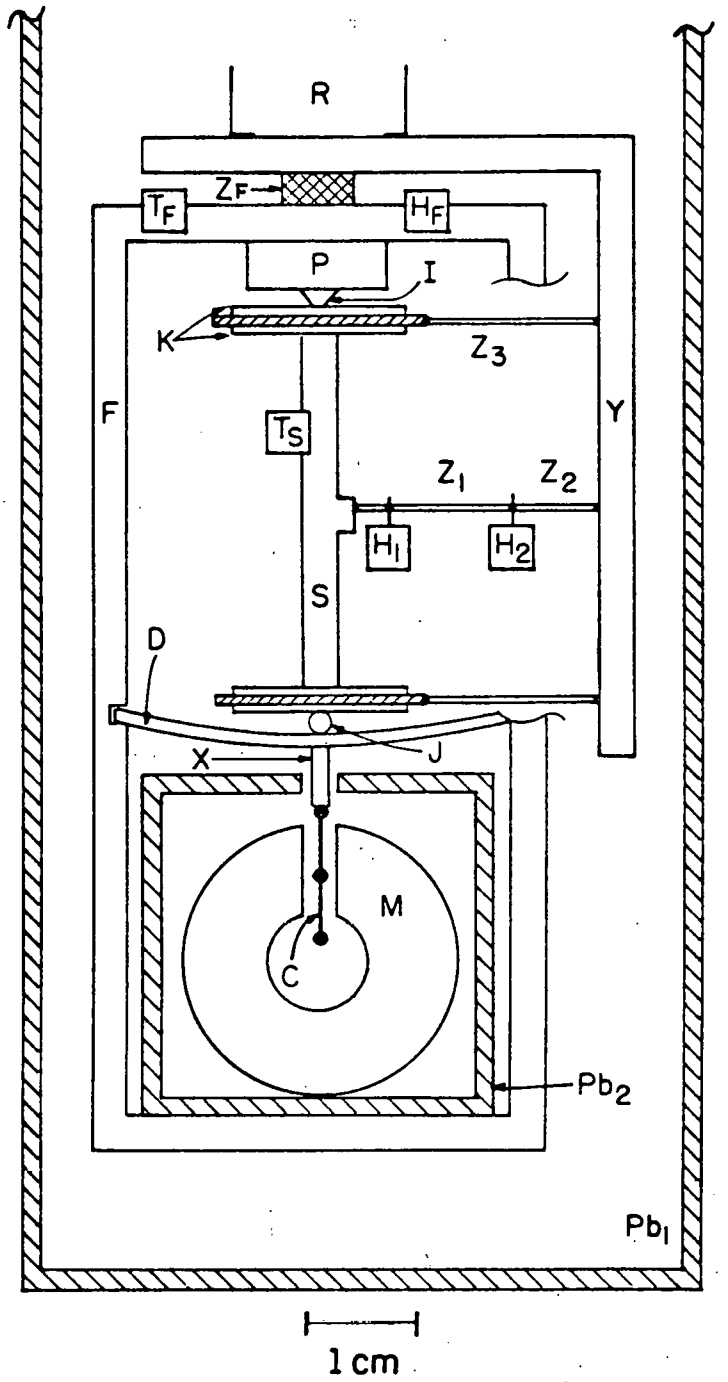

Figure 5. The dilatometer. The drawing is schematic, but dimensions are approximately correct. R-dilution refrigerator; Z-thermal impedances, K-sapphire flats, one of two sets sandwiched over copper foil; D-copper leaf spring; I,J-points of mechanical support; M-permanent magnet; Y-rigid copper yoke; F-rigid copper frame; Pb-lead superconducting magnetic shields; other components and symbols as in Fig. 4.

$(Z_1 + Z_2)C_s$ and C_s is the heat capacity of sample plus addenda. For the Cu sample $\tau_{ext} \approx 1$ sec, which required that the period t_{avg} (cf. Fig. 4) be $\approx$ 20 sec. The thermal link was attached to the copper sample with a copper bolt to ensure good thermal contact. For samples for which this was not possible (e.g., dielectric materials), thin (0.0013 cm) copper foil contacts were bonded using a 1:1 mixture of GE7031 varnish and toluene. The foil was then welded to the heat leak.

The ends of the sample were thermally isolated from the frame so that the sample alone would change temperature during a measurement. A sandwich, placed at each end of the sample, consisted of two 0.036 cm thick, non-paramagnetic sapphire flats and 0.025 cm thick copper foil as shown in Fig. 5. All surfaces were clean and dry to provide maximum thermal impedance,[69] which upon measurement, was found to be a factor of 10^4 higher in magnitude than the boundary resistance attained with the glued thin foil contact. The foils were thermally grounded to the refrigerator through link Z_3 of low thermal impedance so as to shunt any heat passing through the first pair of dry joints.

As a test of thermal isolation, thermometers were placed on several components on the frame and within the shield Pb_2. Any temperature changes were at least a factor of 10^5 smaller than that impressed upon the sample. As a further test, the sample was left in place but decoupled mechanically from the superconducting coil. Changing the temperature of the sample by 80% at any temperature between 0.1 and 10 K produced no SQUID output. Note that, because of impedance Z_2 of Fig. 5, the sample could be maintained at a temperature well above the temperatures of other components.

The temperature T_s and temperature variation ΔT_s of the sample were obtained from a carbon resistance thermometer thermally attached to the sample. The carbon thermometer was calibrated in situ during each run against a germainum resistance thermometer. The germanium thermometer had been calibrated against a set of superconducting fixed points,[70] with interpolation provided by a CMN magnetic thermometer.[71]

Mechanical support of the sample was designed to produce a vertical force on the copper-leaf retaining spring D in Fig. 5. The top mechanical contact I was a point, the bottom contact J was an "edge" provided by a filament of quartz. To replace a sample, the impedance Z_1 was disconnected from the sample, the transducer package P was retracted upwards (using screw adjustments not shown in Fig. 5), and the sample removed. The drive rod X between spring and superconducting coil was a sapphire rod.

The 12-turn superconducting coil was wound in a "figure-eight" configuration (see Fig. 4 and Appendix C) from 0.005 cm diam Nb-Ti wire. The figure-eight design increased the ratio of induced emf/inductance, and reduced sensitivity to spurious fields. The transmission line and any terminals between coil and SQUID were shielded with lead or noibium and were thermally linked only to parts of the refrigerator which were temperature regulated.

The dc level of the SQUID was reset after each time element t_{avg} of Fig. 4. This eliminated long-term drift and, in effect, inserted a low-frequency cutoff of $\lesssim 0.02$ Hz into the pass band of the dilatometer circuit.

The dilatometer could run unattended, and so a practical limit on the signal averaging time for a single datum was overnight allowing $\approx$ 2000 sweeps of duration t_{avg}. This provided a resolution of 2×10^{-4} Å, which ultimately set the minimum temperature to which a given investigation could be carried. Allowing a minimum value of signal-to-noise ratio of $\approx$ 5: $L \times (\alpha(T=T_{min})) \times (0.1\ T_{min}) = 5 \times (2 \times 10^{-4}$ Å). In the case of copper, $T_{min} \approx 0.25$ K. The investigation of copper is described in the next section.

The Thermal Expansion Coefficient of Copper

The linear thermal expansion coefficient of high-purity copper was measured at temperatures between 0.2 and 9 K. The measurement is not presented as a definitive determination, but rather as a test and calibration of the low-temperature dilatometer.

The high-purity, polycrystalline copper had been used previously in a low-temperature measurement of specific heat.[72] A sample was machined to dimensions $0.32 \times 0.32 \times 3.0$ cm^3 plus a side arm as shown by the inset of Fig. 6. The arm allowed the attachment of heater and thermometer without stressing the active portion of the sample. Contaminants were etched from the surface. The etching also revealed crystallites of size $\approx 0.1 \times 0.1 \times 1.0$ cm^3 with long axis oriented parallel to the long axis of the sample as indicated in the inset of Fig. 6. Sample-dependent thermal expansivities have been reported for copper.[73] The sample dependence may result from impurities, strain and/or crystal orientation. No attempt was made to study this problem.

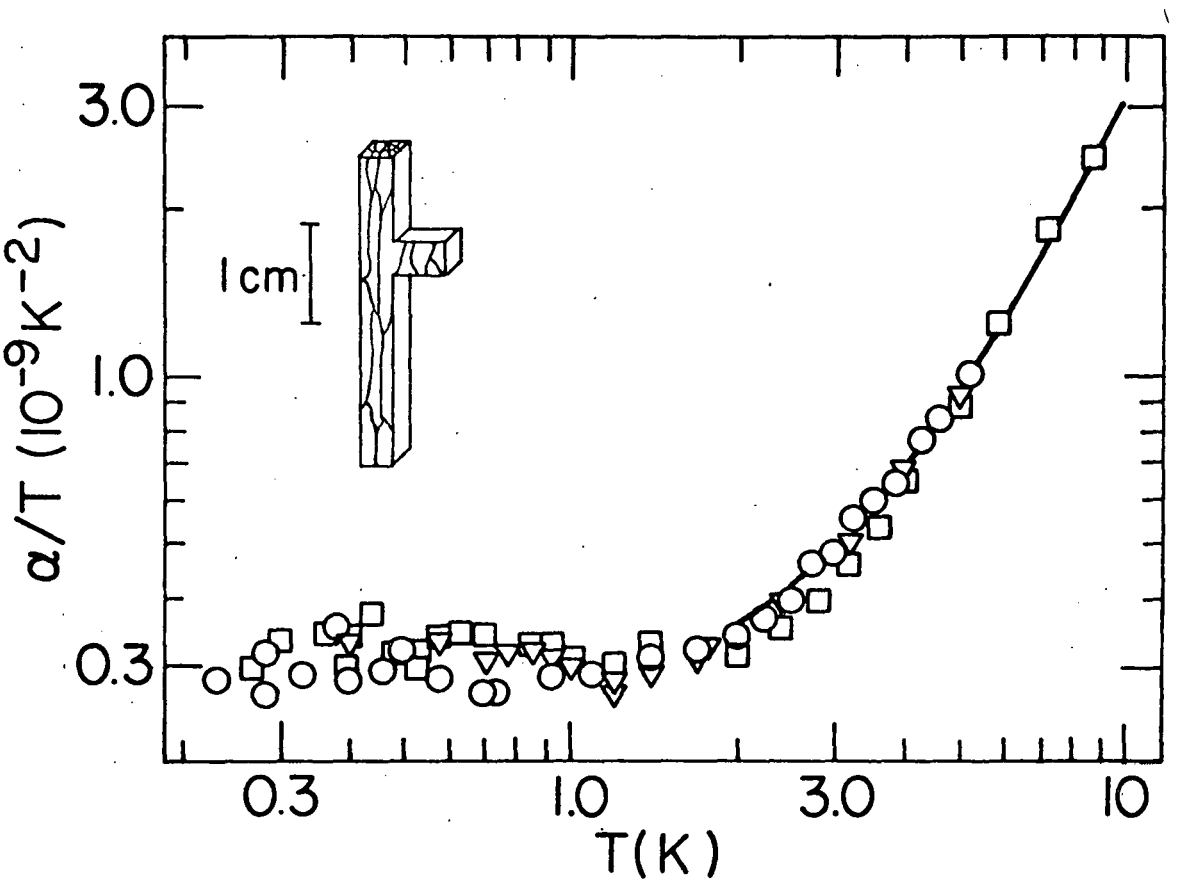

Figure 6. Linear thermal expansion coefficient $\alpha(T)$ of copper, divided by T to emphasize the linear temperature dependence below $\approx$ 1 K. Data from three runs were scaled to agree with the data of Ref. 73 indicated by the solid line. The inset shows the shape of the copper sample, and indicates the alignment of crystallites within the sample.

The data are presented in Fig. 6 as $\alpha(T) / T$ versus T to emphasize the linear temperature dependence for $T \lesssim 1$ K. The sample was run three times, being remounted between each run. Before one run, the superconducting coil was even replaced. Yet the dilatometer output from run to run was the same to ± 6%. Data from the three runs were scaled to provide internal consistency, then the composite was scaled to provide agreement with literature values[73] at temperatures above 2 K as shown in Fig. 6. This procedure constituted the calibration of the dilatometer.[74]

Fitting the copper data to an equation of the form $\alpha(T) = A_1 T^1 + A_3 T^3$ gives $A_1 = 2.9 \pm 0.2$ in units of 10^{-10} K^{-2}, and $A_3 = 2.68 \pm 0.08$ in units of 10^{-11} K^{-4}. The constant A_1 is usually ascribed to conduction electrons, while A_3 arises from the lattice or phonon contribution. A Grüneisen parameter can be defined for each component, $\Gamma_i = 3 B\alpha_i / C_i$. Using the literature value[75] for the modulus, $B = 1.42 \times 10^{12}$ erg/cm^3 independent of T for $T < 10$ K, and measured[72] values for the specific heat C, we obtain $\Gamma_{el} = 1.25 \pm 0.09$ and $\Gamma_{lat} = 1.69 \pm 0.05$ for the electronic and lattice contributions, respectively. The value for Γ_{lat} agrees with published values[73,75] as would be expected, since the $\alpha(T)$ data were scaled to literature values at $T > 1$ K where the lattice contribution dominates. For Γ_{el} there are no data available for comparison. Previous authors[75] have extracted Γ_{el} by curve fitting to data obtained at temperatures above 2 K, obtaining $\Gamma_{el} = 0.91 \pm 0.05$. Theoretical estimates[76] of Γ_{el} range from 0.4 to 1.0.

To summarize Chapter III, a dilatometer was designed and

constructed with a resolution of 2×10^{-4} Å, representing an increase in sensitivity of about a factor of 100 over conventional techniques. Using this apparatus, the linear thermal expansion coefficient $\alpha(T)$ was measured for high-purity copper between 0.25 K and 8.8 K. Although the design of the dilatometer is not claimed to be optimal, it has permitted, for the first time, expansion measurements of copper and furthermore, of amorphous materials, to be pushed to < 1.5 K. Results of investigations on glasses are contained in the next chapter.

IV. RESULTS

The results of linear thermal expansion measurements performed on amorphous dielectrics will be presented in this chapter. The volumetric coefficient of expansion $\beta(T)$ is simply related to the linear coefficient $\alpha(T)$ under the assumption that glasses behave isotropically, $\beta(T) = 3\alpha(T)$. Data are displayed as $\alpha(T)/T^3$ versus T to emphasize departures from a T^3 temperature dependence which would be expected for crystalline dielectrics. Information concerning each of the materials examined is tabulated in Appendix D.

Vitreous Silica: Spectrosil B, Spectrosil WF

The results obtained for two different types of vitreous silica are graphed in Figure 7. Both materials are synthetic, amorphous SiO_2, the differences being in method of manufacture and impurity concentration. Spectrosil B, a flame fused glass, is reported to contain ~1200 ppm OH^- and < 0.1 ppm Ca and Fe while Spectrosil WF, electrically fused, has only 20 ppm OH^- but contains 10 ppm Cl.[77] It was for the difference in hydroxyl ion concentration that both of these materials were examined. Thermal properties of silica apparently dependent upon OH^- concentration have been reported.[14] Thus, it was to be determined whether such inpurity dependence affected thermal expansion.

Below 2 K, the linear thermal expansion coefficient $\alpha(T)$ of Spectrosil B and WF can be fit by the following expressions:

$$(B): \quad ((8.98 \pm 0.43)T^{0.97\pm0.06} + (1.0 \pm 0.2)T^3) \times 10^{-10}\ K^{-1}$$

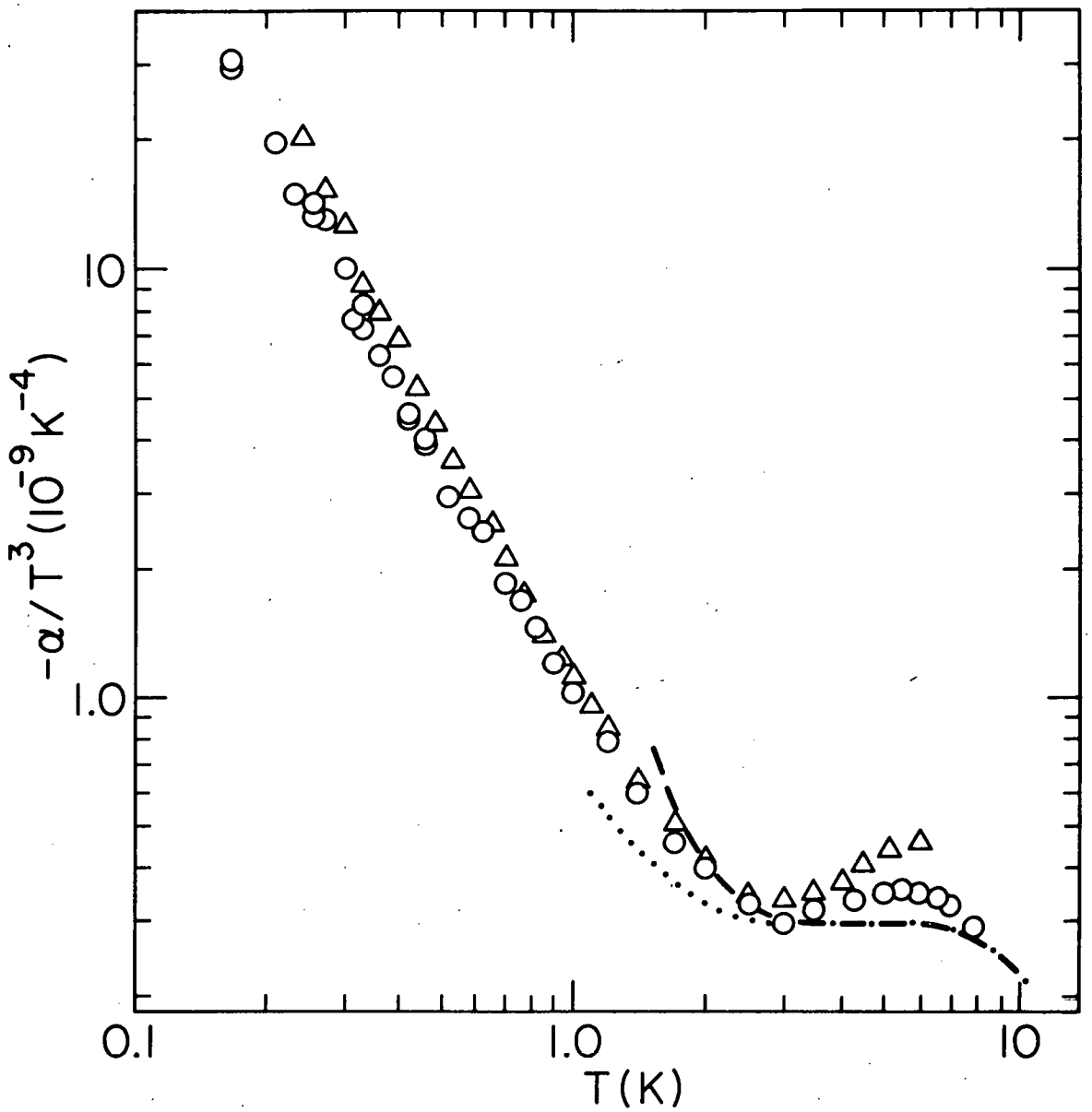

Figure 7. The negative linear thermal expansion coefficient α of two types of vitreous silica, divided by T^3 to emphasize departure from a T^3 phonon contribution. (o) Spectrosil B (data from two independent sets of measurements are indistinguishable), (Δ) Spectrosil WF. Dashed line, data of Ref. 33. Dotted line, data of Ref. 59.

$$(WF): \quad ((9.95 \pm 0.53)T^{1.06\pm0.05} + (1.6 \pm 0.2)T^3) \times 10^{-10}\ K^{-1}$$

The linear coefficients of these two fits are identical to within the ± 10% absolute accuracy of inter-run comparison. Also shown in Fig. 7 are Spectrosil data of Ref. 33 and Ref. 59 for which coefficients of linear temperature dependence equal to $1.05 \pm 0.15 \times 10^{-9}\ K^{-1}$ and $0.441 \times 10^{-9}\ K^{-1}$, respectively, were extracted.

Above 1 K, a bump in $-\alpha/T^3$ is visible for both samples, peaked at roughly 5 K. This feature is not reported in previous work.[33,59] It is possible, therefore, that it is an artifact of the measuring technique. This is doubtful however, as no such bump is seen for any other material investigated by the same technique. The peak may be somehow connected with a bump in $C(T)/T^3$ (of unknown origin) which occurs at slightly higher temperatures.[18,31]

Amorphous Polymers: SC5, PMMA

Thermal and acoustic properties characteristic of the glassy state have been observed in amorphous polymers below 1 K.[11,17,59] Previous work[11] on such a material, Scotchcast 5 epoxy resin (SC5),[78] made available an amorphous sample well characterized with respect to specific heat and sound velocities. For this reason, expansion measurements were made on a sample of SC5 cut from the same block used in Ref. 15. Previous thermal expansion measurements performed above 1.5 K on another glassy polymer polymethylmethacrylate (PMMA) were interpreted as possible indication of anomalous $\alpha(T)$ below 1 K.[59] Thus, thermal expansion of PMMA was measured also, on a sample cut from stock Plexiglas.

The data, plotted in Fig. 8 as $+\alpha/T^3$ versus T, are, in contrast to that of silica glass, positive and lacking in a distinct low temperature linear temperature dependence. Visible for SC5 at $T \lesssim 0.5$ K is the slight suggestion of a positive linear contribution to $\alpha(T)$, about a factor of 10 less in magnitude than that of vitreous silica. At this same temperature, $\alpha(T)$ of PMMA is positive and proportional to $\sim T^5$. Prediction[59] of $\alpha(T)$ becoming negative at ≈ 1 K for PMMA is not borne out experimentally. Favorable agreement with data of Ref. 59 is obtained above 1.5 K, despite differences in origin and thermal history of the PMMA samples. It should be noted that, despite differences below 1 K, the expansion coefficients of SC5 and PMMA are similar in magnitude and temperature dependence above ~2 K.

Arsenic Trisulfide, As_2S_3

Plotted in Fig. 8 are data obtained for a sample of chalcogenide glass, As_2S_3. The material itself is a twin sample to that examined in reference 42. It is therefore not surprising that agreement in $\alpha(T)$ with Ref. 42 is obtained above ~3 K. The data are positive and similar in magnitude to the amorphous polymers above 1 K, and approximately cubic in temperature at lower temperatures. There is no evidence to support the speculation that $\alpha(T)$ should become negative at ~1.2 K.[42] This conjecture was based on a fit to data between 2 and 5 K, from which a negative linear contribution to $\alpha(T)$ was extracted. Clearly demonstrated is the risk involved in extrapolation of $\alpha(T)$ to temperatures below 1 K.

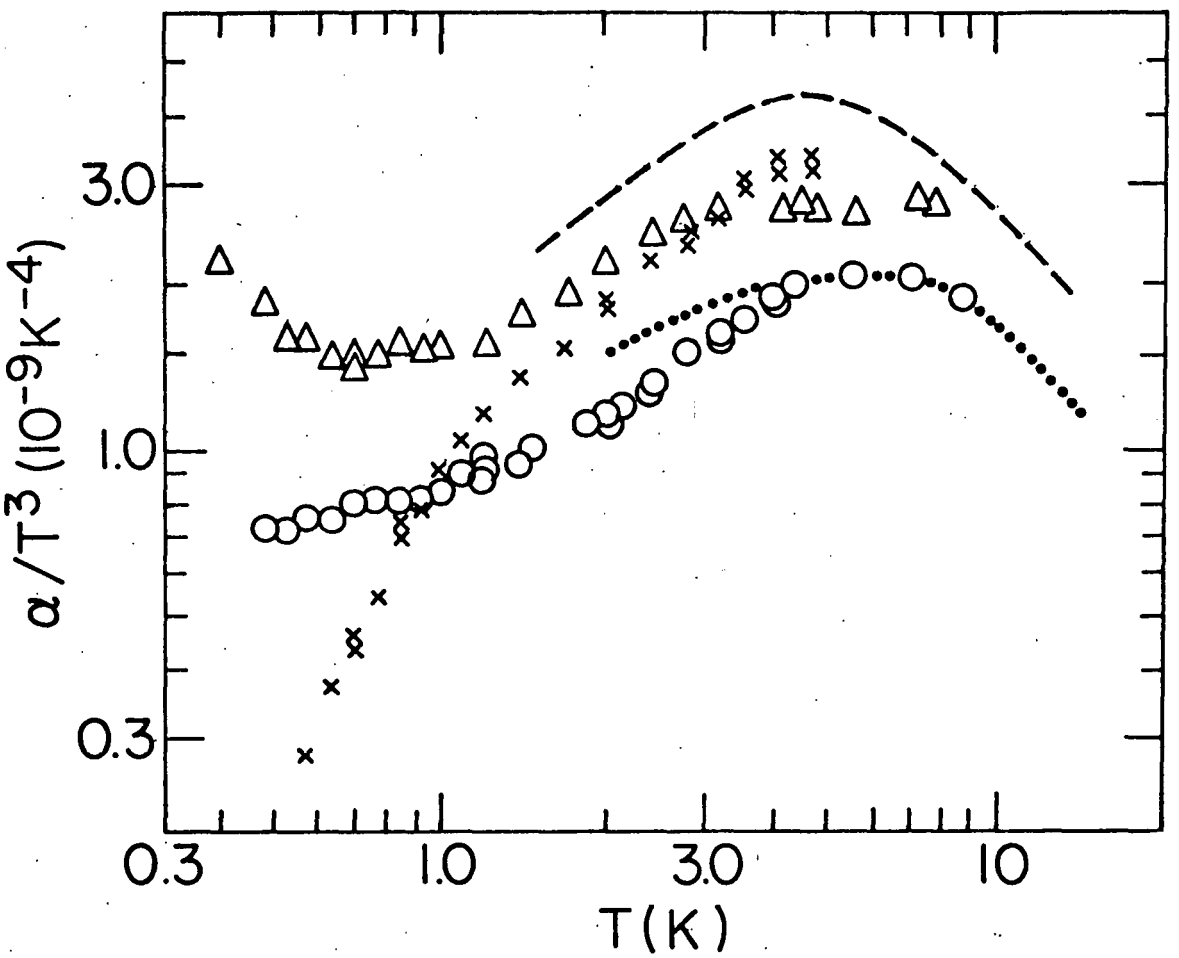

Figure 8. The positive thermal expansion coefficient α (divided by T^3) of (o) glassy As_2S_3, (×) PMMA and (△) epoxy SC5. Dashed line, data of Ref. 59 for PMMA. Dotted line, data of Ref. 42 for As_2S_3.

Cubic Zirconia, $ZrO_2 : Y_2O_3$

A crystalline material ZrO_2, stabilized in a cubic structure by addition of 16% Y_2O_3, has shown preliminary evidence of glass-like properties at low temperatures.[31,79] This behavior has precedent in other crystalline materials[31] and motivated the investigation of thermal expansion of cubic zirconia. The data illustrated in Fig. 9 show a distinct linear temperature dependence analogous to that observed in vitreous silica, but of opposite sign and a factor of 10 smaller in magnitude, $\alpha(T) = (1.0T + 0.045T^3) \times 10^{-10}\ K^{-1}$.

To summarize the results presented in Chapter 4, thermal expansion of several glassy materials of widely differing composition and structure has been measured. While $\alpha(T)$ of vitreous silica was demonstrated to be negative, independent of OH^- concentration and linear in temperature below 1 K, $\alpha(T)$ of two glassy polymers and As_2S_3 were positive and varied in temperature at least as fast as T^3. The thermal expansion coefficient of cubic zirconia exhibited a linear temperature dependence at low temperatures. These results can be displayed somewhat differently, by extracting a (temperature dependent) Grüneisen parameter. This task, and further analysis, are taken up in Chapter V.

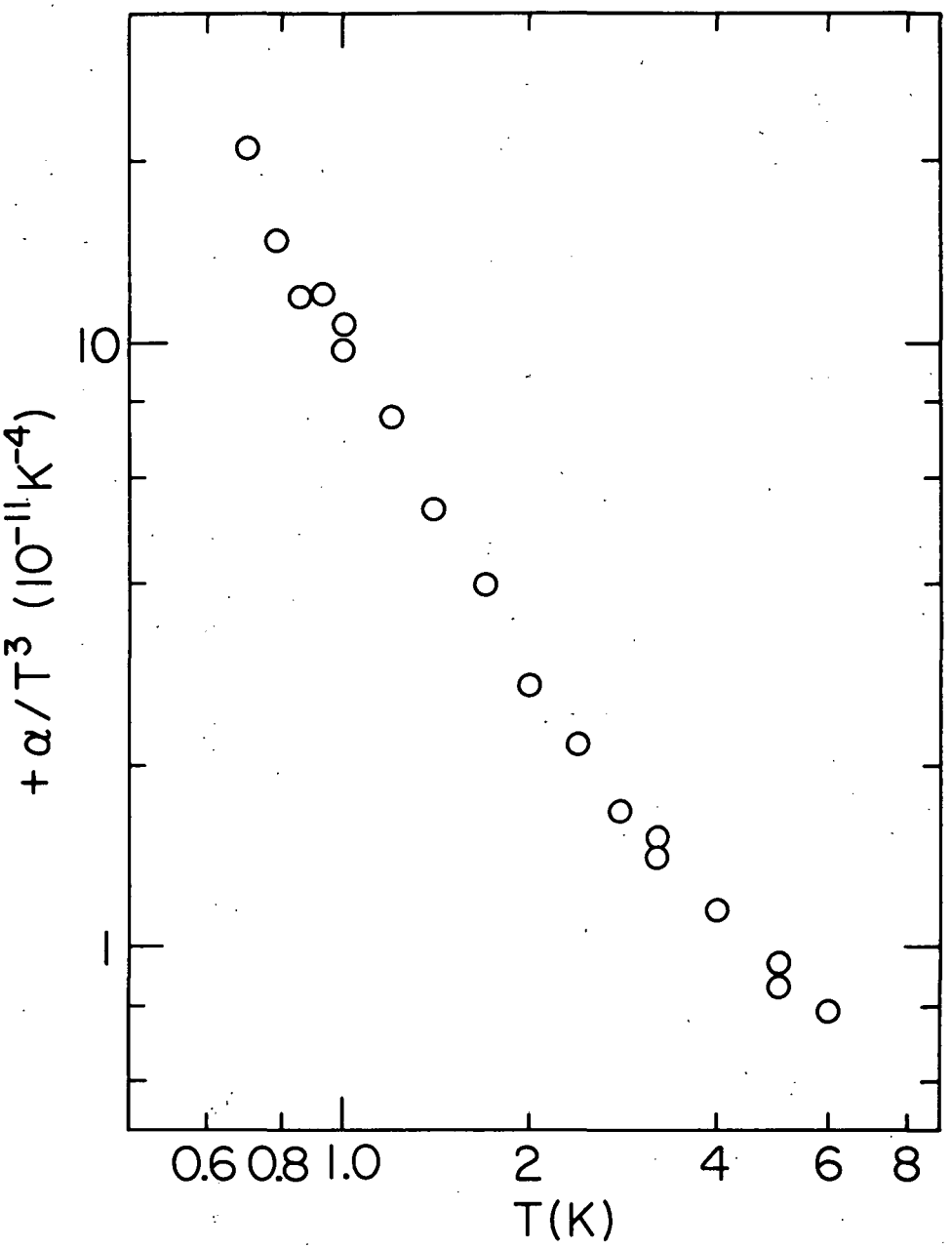

Figure 9. The positive thermal expansion coefficient α (divided by T^3) of cubic zirconia containing 16% molar Y_2O_3.

V. DISCUSSION

Introduction

Results presented in Chapter IV can be interpreted in terms of the Grüneisen equation of state, $\beta B = \Gamma C$. The Grüneisen parameter Γ is determined by measured quantities: thermal expansion coefficient $\beta(T)$, specific heat C, and bulk modulus $B = \rho(v_\ell^2 - \frac{4}{3}v_t^2)$. (Mass density ρ and longitudinal and transverse sound velocities v_ℓ and v_t are taken as constant over temperatures of interest.) Γ, by this definition, is a temperature-dependent quantity. For each amorphous material for which $\beta(T)$ was measured, Γ is plotted as a function of temperature in Figs. 10 and 11. Despite suggestions that $\Gamma(T \to 0) \approx -20$, universal to all glasses, it is evident from Figs. 10 and 11 that Γ for amorphous materials can be positive, negative, large or small. Understanding of this behavior within the framework of the phenomenological theory used for TLS can be accomplished by relaxing a simplifying assumption of the model.

Grüneisen Parameters

Vitreous Silica

Two types of vitreous silica were examined, Spectrosil B and Spectrosil WF, containing $\approx$1200[33,77] and 20[77] ppm OH^- impurities respectively. For both samples, thermal expansion and specific heat[15] were measured. Using a value of bulk modulus $B = 3.6 \times 10^{11}$ erg/cm^3 calculated from measured sound velocities,[15] Grüneisen parameters for

each material were calculated and appear plotted in Fig. 10. The difference in Γ at low temperatures for these two glasses, -40 for Spectrosil B and -60 for Spectrosil WF at 0.2 K, is striking in light of the similarity in $\beta(T)$ between the two as described in Chapter IV, and derives mainly from the difference in specific heats: C(Spectrosil B) = $(46.0 \pm 2.3)T^{1.35\pm0.05}$ below 0.6 K[15] while C(Spectrosil WF) = $30.5T^{1.28\pm0.04}$ below 0.5 K.[80] A variation in specific heat of vitreous silica with hydroxyl ion content has been investigated previously[14] using Suprasil (1200 ppm OH^-) and Suprasil W (< 1.5 ppm OH^-). At 0.1 K, the ratio of the specific heat C of Suprasil to that of Suprasil W was $\approx$1.3, which agrees with the ratio of C of Spectrosil B to that of Spectrosil WF at the same temperature. In addition, Suprasil and Spectrosil B have identical specific heats.[43] The conclusion drawn in the investigation of Suprasil was that the addition of OH^- groups to vitreous silica leads to an increase in the number of TLS having "very small splitting," i.e. < 1 K in energy.[14] This reasoning may be extended to the Spectrosil system. In view of the similarity of thermal expansion coefficients of Spectrosil B and WF however, it must be concluded that the total contribution of these OH^--related states to expansion is minimal. In other words, the Grüneisen parameter of the collection of low energy OH^--related states is small, perhaps falling in the normal range of ~1 to 3.

Also appearing in Fig. 10 is a plot of Γ, measured directly by means of an adiabatic compression experiment, on a sample of Vitreosil.[60] By measuring changes in temperature resulting from a periodic, imposed

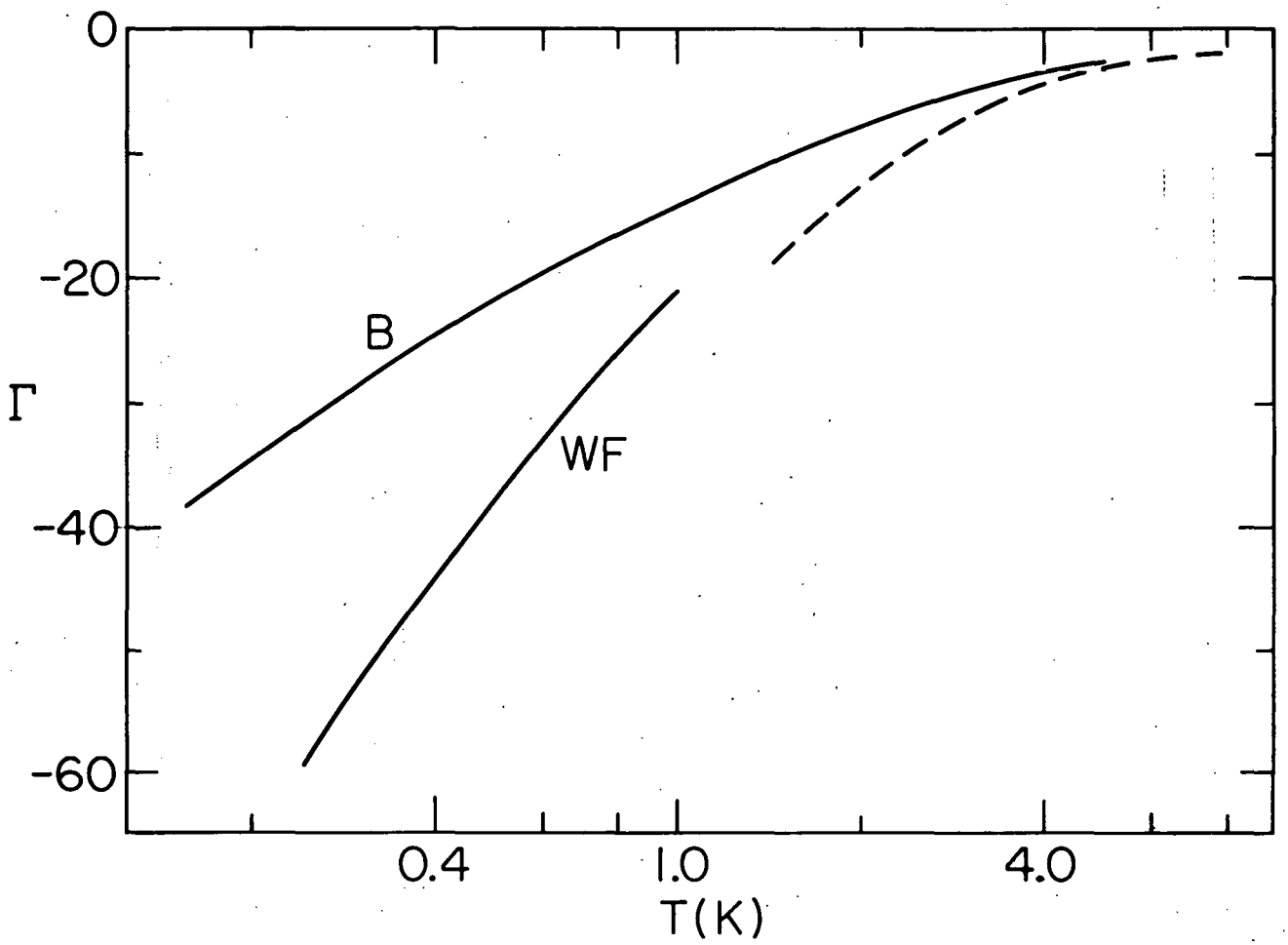

Figure 10. The Grüneisen parameters Γ for two types of vitreous silica, Spectrosil B and Spectrosil WF. Dashed line, direct measurement of Γ for vitreous silica from Ref. 60. (Note: $\Gamma < 0$)

strain, Γ was determined as $\Gamma = -\partial \ell nT / \partial \ell nV \big|_S \equiv \beta B/C$. Down to ~1.5 K, Γ of Vitreosil (vitreous silica) appears qualitatively similar to Spectrosil.

Amorphous Polymers

The results of thermal expansion of two amorphous polymers, polymethylmethacrylate (PMMA) and Scotchcast 5 epoxy (SC5), indicate behavior quite different from vitreous silica. Grüneisen parameters for each polymer, plotted in Fig. 11, are positive and small over the temperature range of 0.5 to several K (availability of C(T) data limits calculation of Γ of SC5 to $T < 2$ K). In the case of SC5 at low temperatures, Γ appears to tend toward a constant value of $\approx +0.8$. This conclusion assumes that for SC5, the temperature dependence of $\beta(T)$ does indeed become linear below 0.5 K. Γ of PMMA does not converge to a constant value but instead continues to decrease in magnitude to $\approx +0.2$ at ~0.5 K. Speculation as to a low temperature limiting value of Γ for PMMA must rely on extrapolation of $\beta(T)$ below 0.5 K. The difficulty of such a task together with a lack of very low temperature C(T) data renders such guesswork meaningless. On this basis, estimates[59] of $\Gamma \rightarrow -16$, using $\beta(T)$ data above 1.5 K only, should be regarded with suspicion. Thus, despite the typical glassy signature exhibited by both polymers,[17,15] universal thermal expansion behavior is not observed.

Arsenic Trisulfide

The Grüneisen parameter for amorphous As_2S_3 is plotted in Fig. 11. As is the case for the polymers, Γ is positive and ≈ 1, a value

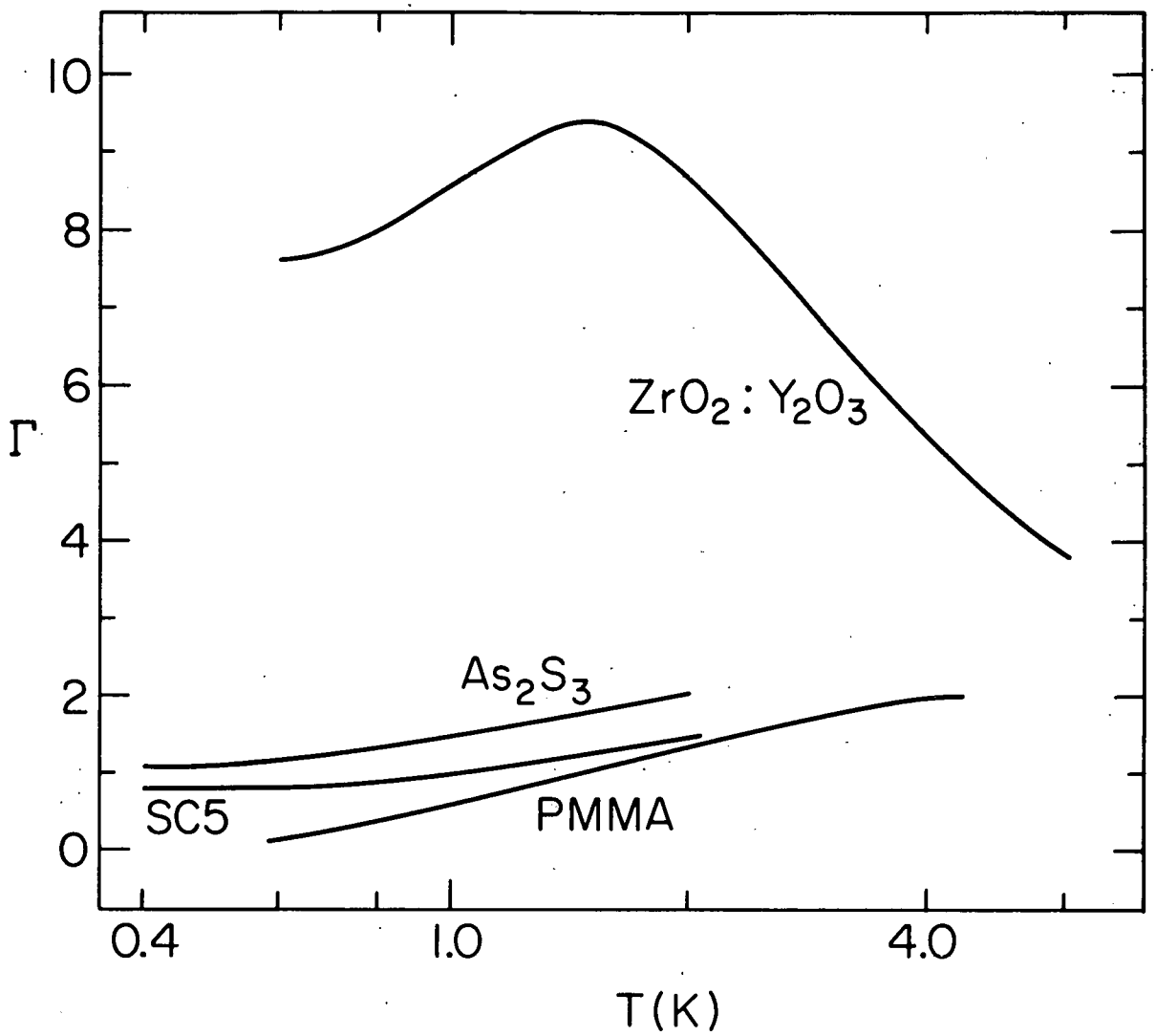

Figure 11. The Grüneisen parameters Γ for cubic zirconia, glassy As_2S_3, SC5 and PMMA. (Note: $\Gamma > 0$)

typical of most crystalline materials. Indications of low temperature anomalies in magnitude, temperature-dependence and sign are absent. Present observations show no evidence of $\Gamma \rightarrow -25$ as implied by an investigation above 1.5 K.[42]

Cubic Zirconia

Cubic zirconia (ZrO_2 stabilized in the cubic phase with the addition of 16 molar % Y_2O_3) has displayed many of the same low-temperature properties as glasses despite its crystalline structure. Disorder in this material, which might derive from the presence of Y_2O_3, has been proposed as an explanation of glass-like behavior. Thermal expansion results, together with measured specific heat,[81] yield a Grüneisen parameter which is plotted in Fig. 11. Γ at low temperatures is large and positive. Γ reaches a maximum of ~9 at 1.5 K corresponding to a slight depression apparent in a plot of C/T^3.[81] At temperatures below 1 K, Γ decreases slowly, proportional to $T^{0.2}$.

Thermal Expansion and the TLS Model

The Grüneisen model expresses the intimate relationship between specific heat and thermal expansion. TLS with energy $E \sim kT$ can accept energy from the phonon bath at temperature T and thus contribute to the heat capacity of the system. Specific heat C is a measure of the number of states (per volume) which can undergo excitation--and store energy--with changes in temperature δT. Upon excitation, these same states participate in thermal expansion by changing their effective volume. A

parameter relating the change in volume of the i-th TLS to changes in energy is $\Gamma_i = \partial \ell n E_i / \partial \ell n V$. Γ_i, together with heat capacity C_i, determines the total Grüneisen parameter Γ due to the TLS, $\Gamma = \sum_i \Gamma_i C_i / \sum_i C_i = \beta B/C$, in which β = thermal expansion coefficient, and B = bulk modulus.

The calculation of specific heat in the TLS model does not require detailed structural information. A two-level-system has a heat capacity dependent only on E, given by Eq. II-9. Integration over an energy-independent density of states yields a specific heat, linear in temperature, without reference to energies ϵ and Δ or deformation potentials M and D (defined in Chapter II, Eqs. 2, 6 and 7). Once the density of states is known however, measurement of ultrasonic dispersion permits estimation of both M (through resonant scattering--and also, through phonon echoes) and D (through relaxation scattering).[38] More precisely, by measuring the mean-free-path due to relaxation attenuation, an estimate of D^2 is obtained from which $|D| \approx$ lev is implied.[38] For the purpose of modelling the observed ultrasonic attenuation, a value of D constant for all TLS is used successfully.[38]

From this stage, an estimate of the Grüneisen parameter can be obtained by noting that

$$|\Gamma_i| = \frac{\partial \ell n E_i}{\partial \ell n V} = \frac{1}{E_i}\left(\frac{\epsilon}{E}\frac{\partial \epsilon}{\partial e} + \frac{\Delta}{E}\frac{\partial \Delta}{\partial e}\right)_i = \frac{D_i}{E_i} \qquad \text{V-1}$$

in which

$$\frac{\partial}{\partial \ell n V} \equiv \frac{\partial}{\partial e}$$

Since $\Gamma = \sum_i \Gamma_i C_i / \sum_i C_i$, in which the sum is over all TLS, and D is a constant, $|\Gamma| = (D \sum_i C_i / E_i) / (\sum_i C_i) \approx 10^4/T$. Γ is predicted to be large and inversely proportional to temperature. This is not the behavior observed in Figs. 10 and 11 for any material. All $|\Gamma|$ at ~1 K are $\lesssim 15$ and the strongest temperature dependence is observed in vitreous silica, $\Gamma \propto -T^{-0.4}$. Questionable is the assumption that D ≈ 1eV for all states. A cancellation among contributions of individual TLS to thermal expansion must occur as has been discussed previously.[39]

A simple argument for cancellation can be made by introducing D = D(E) whereby results of ultrasonic experiments and results of the present thermal expansion measurements may be reconciled. By imagining the i-th TLS as being an isolated defect within a host matrix, subject to a local bias strain e_i, the energy of this defect as a function of strain may be written in expanded form as

$$E_i(e) = E_{0i} + \left.\frac{\partial E}{\partial e}\right|_{e_i} (e - e_i) + \frac{1}{2}\left.\frac{\partial^2 E}{\partial e^2}\right|_{e_i} (e - e_i)^2 + \ldots \qquad \text{V-2}$$

in which $(e - e_i)$ is the instantaneous local strain. Neglecting the constant term, and letting $D = \left.\frac{\partial E}{\partial e}\right|_{e_i}$, $E_i = D(e - e_i)$ to first order in strain. D need not be uniform over the population of TLS since the random structure of the glassy host could provide various values of e_i as well as completely different environments[38] resulting in a variety of forms of ∂E/∂e. Consequently, a distribution in values of D for a

given energy can arise. For convenience, a Gaussian distribution of the form

$$n(D(E)) = \frac{n(E)}{\sqrt{2\pi}\,\sigma} \exp - \left[\frac{(D - D_{avg}(E))^2}{2\sigma^2} \right] \qquad V\text{-}3$$

is adopted, in which $D_{avg}(E)$ is the mean value (center) of the distribution as a function of energy E, σ is the width of the distribution and $\int_{-\infty}^{\infty} n(D(E))\, dD = n(E) = n_o$, a constant, for normalization (see Fig. 12).

The effect of a distribution in D on calculation of ultrasonic attenuation is determined by the relative magnitudes of D_{avg} and σ. Since, in the expression for the relaxation mean-free-path, the deformation potential appears as D^2, integration over all states produces $\langle (D(E))^2 \rangle$. The square root of this averaged D^2, or D_{rms}, must be $\approx$1eV, as observed. Using the Gaussian distribution,

$$D_{rms}(E) = \int_{-\infty}^{\infty} D^2(E)\, n(D(E))\, dD = (\sigma^2 + (D_{avg}(E))^2)^{1/2} \qquad V\text{-}4$$

If $\sigma \gg D_{avg}$, $D_{rms} \approx \sigma(1 + (D_{avg}^2/2\sigma^2)) \approx \sigma$, which may be chosen to be energy-independent and $\approx$1eV. Since $\int_{-\infty}^{\infty} n(D(E))\, dD = n_o$ = constant, and σ is fixed, the shape of the distribution curve is determined, independent of E. Only by sliding the Gaussian along the D axis may a variation be obtained as a function of TLS energy E.

The effect of a distribution of this nature on thermal expansion must be considered in light of the present data. The Grüneisen parameter

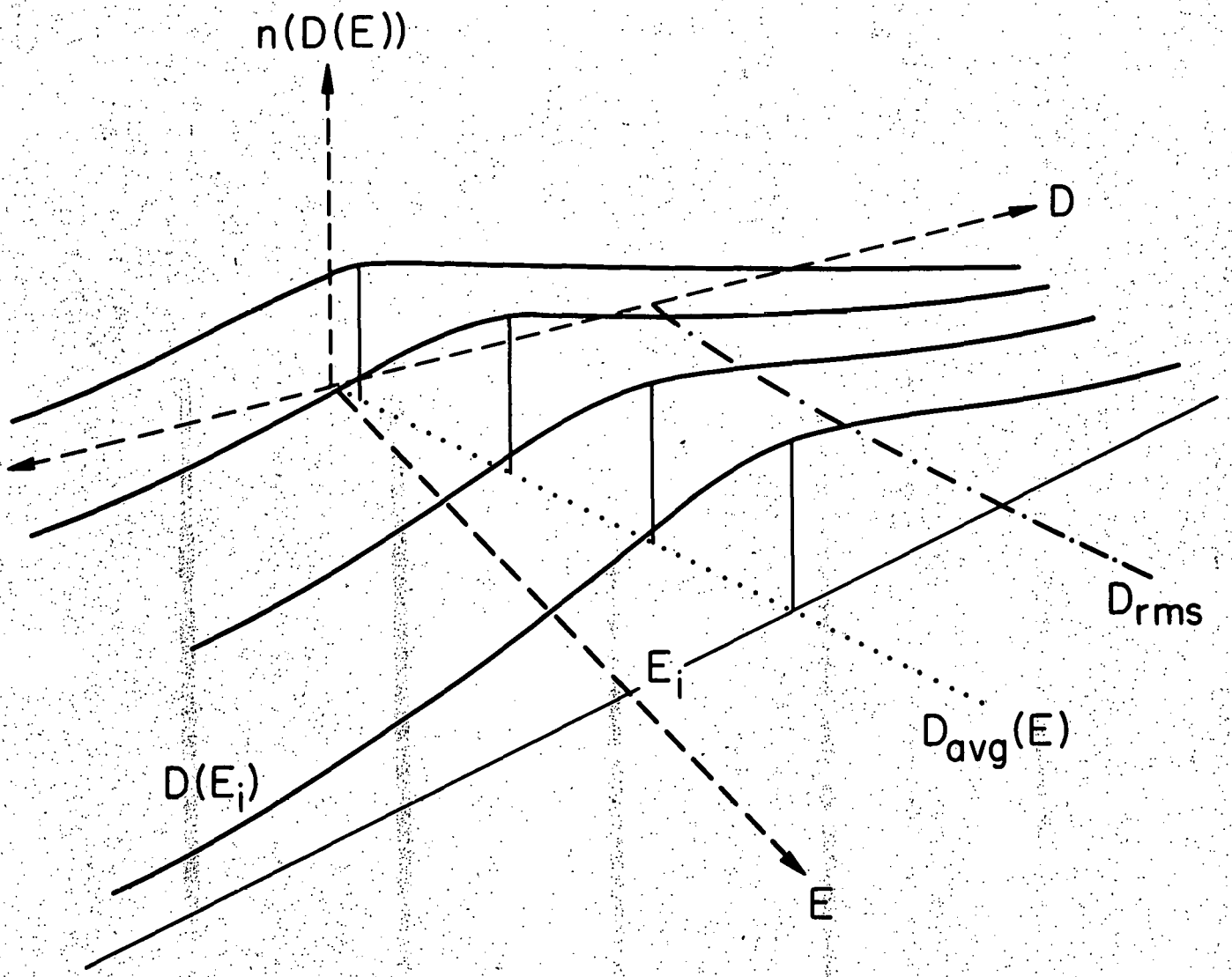

Figure 12. Distribution n(D(E)) as a function of deformation potential D and energy E. For a given energy E_i, $n(D(E_i))$ is centered about $D_{avg}(E_i)$. The width σ of $n(D(E_i))$, much greater than $D_{avg}(E_i)$, is not shown to scale.

Γ can be expressed as a function of E:

$$\Gamma(E) = \int_{-\infty}^{\infty} \Gamma(D(E))\, n(D(E))\, dD \;/\; \int_{-\infty}^{\infty} n(D(E))\, dE \qquad \text{V-5}$$

in which

$$\Gamma(D(E)) = -D(E) / E$$

$$\Gamma(E) = -\frac{1}{E} \int_{-\infty}^{\infty} D\, n(D(E))\, dD \;/\; n(E) = -\frac{D_{avg}(E)}{E} \qquad \text{V-6}$$

Using Eq. V-6, $\Gamma = \sum_i \Gamma_i C_i \;/\; \sum_i C_i$ becomes

$$\Gamma = \int_0^{\infty} dE\, n(E)\, \frac{-D_{avg}(E)}{E}\, C(E) \;/\; \int_0^{\infty} dE\, n(E)\, C(E) \qquad \text{V-7}$$

(cf., $\Gamma = (-D \sum_i C_i / E_i) \;/\; (\sum_i C_i)$). Thus, Γ is sensitive to D_{avg} which may be positive, negative, dependent on E, and of any magnitude as long as the condition $(D_{avg})^2 < 2\sigma^2$, imposed by ultrasonic data, is satisfied. In short, $|D_{avg}| \ll D_{rms}$ implies that some of the TLS at a given energy expand while others contract upon excitation.

Speculation on particular distributions of deformation potential D can be made using the data presented in Chapter IV. As an example, let $D_{avg}(E) = D_{avg}(E/E_o)^{\nu}$ in which $E_o/k = 1$ K and $\nu = 0 \rightarrow 2$. Assuming a constant energy distribution of TLS, $n(E) = n_o$, and using Eq. II-9 for C(E), Eq. V-7 becomes

$$|\Gamma| = \frac{\int_o^\infty dE \, \frac{D_{avg}(E)}{E} \, k \left(\frac{\beta E}{2} \operatorname{sech} \frac{\beta E}{2} \right)^2 n_o}{\int_o^\infty dE \, k \left(\frac{\beta E}{2} \operatorname{sech} \frac{\beta E}{2} \right)^2 n_o} \qquad \text{V-8}$$

$$= (\text{constant}) \, D_{avg} \, (kT)^{\nu-1} \, E_o^{-\nu} \propto T^{\nu-1}$$

in which

$$(\text{constant}) = (2^\nu 6/\pi^2) \int_o^\infty dx \, x^{\nu+1} \operatorname{sech}^2 x \sim 0(1).$$

For the Spectrosil samples, $\Gamma(T = 0.2\ K) \propto T^{-0.4}$ implying $\nu \approx 0.6$ while $D_{avg} \approx -20$ in units of K or $\approx -2 \times 10^{-3}$ eV. Since $D_{rms} \approx$ 1eV, the width of the distribution $\sigma = ((D_{rms})^2 - (D_{avg})^2)^{1/2}$ is also ≈1eV. Therefore, the condition $(D_{avg})^2 \ll 2\sigma^2$ is satisfied, i.e., the experimental magnitudes and temperature dependences of both thermal expansion and ultrasonic attenuation can be obtained using the Gaussian distribution of Eq. V-3. A broad distribution in D reflects the random nature of the TLS-phonon coupling within a glass. An important feature of the distribution is the center value D_{avg} which may be skewed to either positive or negative values of D. The tendency for TLS to have, for example, negative D, as is the case for Spectrosil, might indicate the presence of a preferred configuration of TLS with negative Grüneisen parameter. How, if at all, this configuration is related to other modes in vitreous silica, having negative Γ and predominant at higher temperatures, is not clear. Of the materials observed, however, those with negative (positive)

Γ at temperatures above 1 K, attributed to phonon modes, had negative (positive) Γ at low temperatures.

The OH^- related states, which seemed not to contribute to thermal expansion, may have $D_{avg} = 0$ and/or $\sigma = 0$, i.e., upon excitation, they might suffer complete cancellation or simply might have a small Γ. On the other hand, in the comparison of Spectrosil B and Spectrosil WF, it is likely that the two samples differed in thermal history as well as OH^- content. If this or another difference influenced $\beta(T)$, it would be impossible to determine the precise effects of hydroxyl ions. The question of hydroxyl ion concentration was pursued no further than to demonstrate that OH^- ions were not solely responsible for the anomalous $\beta(T)$ in vitreous silica.

PMMA and SC5 exhibited $\Gamma \sim +1$. In terms of distributions of D, this would imply a value of $D_{avg} \lesssim 10^{-4}$ eV. Evidence of anomalous $\beta(T)$ at the lowest temperatures investigated might indicate behavior similar to SiO_2 but so much smaller as to be masked by phonons for temperatures above 0.5 K. Such may have been the case for As_2S_3, also. It may be that small D_{avg} is characteristic of "softer" materials, $B \lesssim 10^{11}$ erg/cm^3 (Appendix D), although the reason for this is not apparent. In contrast, cubic zirconia exhibiting a large, positive Γ could have $D_{avg} \sim +10^{-3}$ eV. In a crystalline structure, TLS with uniform structure may occur, broadened in energy E and deformation potential D by strain interactions.[55] Nevertheless a study of zirconia versus Y_2O_3 concentration is required to establish a trend.

It is important to note that while the hypothesis of a broad and skewed distribution in D can reconcile ultrasonic and thermal expansion data, it is still very difficult to establish a microscopic picture of a TLS in any glass. The occurrence of $D_{avg} \neq 0$ may reflect a preference--however slight--for a particular TLS structure within a given material. In the language of the tunneling states model, a negative (positive) D_{avg} implies that compression of a TLS renders a tunneling site more (less) symmetric and/or reduces (enhances) overlap. The distribution in D invoked here to explain thermal expansion data adds complexity to the TLS model. Despite this shortcoming, it allows resolution of a discrepancy in predictions of the TLS model with experimental observations.

Conclusions

In conclusion, the major results of this work are summarized.

Thermal expansion measurements on amorphous materials have, for the first time, been extended below 1.5 K. A SQUID dilatometer, which made possible these measurements, was developed and demonstrated to have resolution of $\approx 2 \times 10^{-4}$ Å in changes of sample length (strain, $\delta\ell/\ell \approx 7 \times 10^{-13}$). Accuracy of ±10%, from run to run, was determined by repeated measurements on high purity copper which served also as an absolute calibration. The copper data between 0.3 K and 2 K was presented for the first time and allowed a determination of the electronic Grüneisen parameter.

Measurements of the linear thermal expansion coefficient $\alpha(T)$ of two types of vitreous silica, two amorphous polymers, amorphous As_2S_3

and cubic zirconia were then carried out. Results showed that $\alpha(T)$, ($\beta(T) = 3\alpha(T)$), of glasses could be positive or negative, large or small. Grüneisen parameters Γ were then calculated for these glasses, demonstrating that the magnitude, temperature dependence and sign of Γ are not uniform among all glasses as has been found for other thermal and acoustic properties. It was further discovered that $\beta(T)$ of vitreous silica was not sensitive to the concentration of hydroxyl ions (OH^-). Analysis of thermal expansion data above 1 K would be complicated by the phonon contribution as is the case with specific heat. A bump in $-\alpha/T^3$ observed in vitreous silica, as well as the apparent similarity in $\alpha(T)$ of SC5, PMMA, and As_2S_3 might be useful in understanding the behavior of glasses at $T > 1$ K. This higher temperature analysis was not attempted in the present effort.

Explanation for material dependent $\beta(T)$ and Γ, in the context of the two-level-states model, was accomplished through use of a distribution in deformation potentials.[82] This permitted interpretation of ultrasonic behavior, dependent on the root-mean-square value of the distribution, and interpretation of thermal expansion, dependent on the mean value of the distribution, to remain consistent within the TLS model. That TLS should have a slight preference, when excited, to expand in certain materials and contract in others constitutes the first evidence of qualitative material-dependent glassy behavior.

Further experiments using thermal expansion at low temperatures to probe glassy properties are suggested by this work. A systematic $\beta(T)$ study of a crystalline or glassy material as a function of impurity

level could determine the role of the impurity in thermal expansion. Examples of such systems (under investigation) are ZrO_2 containing x% Y_2O_3 and SiO_2 containing x% K_2O. Improvement of the absolute accuracy of the SQUID dilatometer would permit meaningful inter-run comparison of thermal expansion results. Focus on improvement of the reproducibility of the piezoelectric calibration element (as mentioned in Chapter III) would permit these studies.

APPENDIX A

LOW-PASS FILTER

Large amplitude, high frequency vibration of the detector coil relative to the permanent magnet produced noise in the SQUID circuit, often exceeding the maximum slewing rate of the SQUID sensor. A low-pass filter placed between the detector coil and SQUID served to attenuate the vibrational noise. The following criteria were followed in designing the filter: (1) filter must provide enough attenuation for frequencies $\gtrsim$ 1 Hz to allow SQUID to operate in locked mode, (2) filter must produce no distortion of the thermal expansion signal, (3) filter must withstand repeated thermal cycling.

Tests were made using one, two and three stage filters with characteristic cut-off frequencies between 0.5 and 5 Hz. Only a three stage filter provided adequate attenuation at troublesome natural vibration frequencies of the refrigerator and apparatus (5 to 500 Hz). A schematic of the filter is shown in Fig. 13. The current I_4, coupled directly into the SQUID via L_4, is a sum of currents due to flux changes in the detector coil $I_4(\phi)$ and Johnson noise in each resistor $I_4(V_j)$. (Note that one and two stage filter characteristics can be obtained by setting appropriate values of $L \to 0$, $R \to \infty$.)

The final version of the filter is pictured in Fig. 14a. Inductors are oriented almost perpendicular to one another to minimize cross-talk. Each inductor is 87 turns of 0.010 cm diam niobium wire (including insulation) on a hollow core of diam 0.16 cm yielding on inductance of

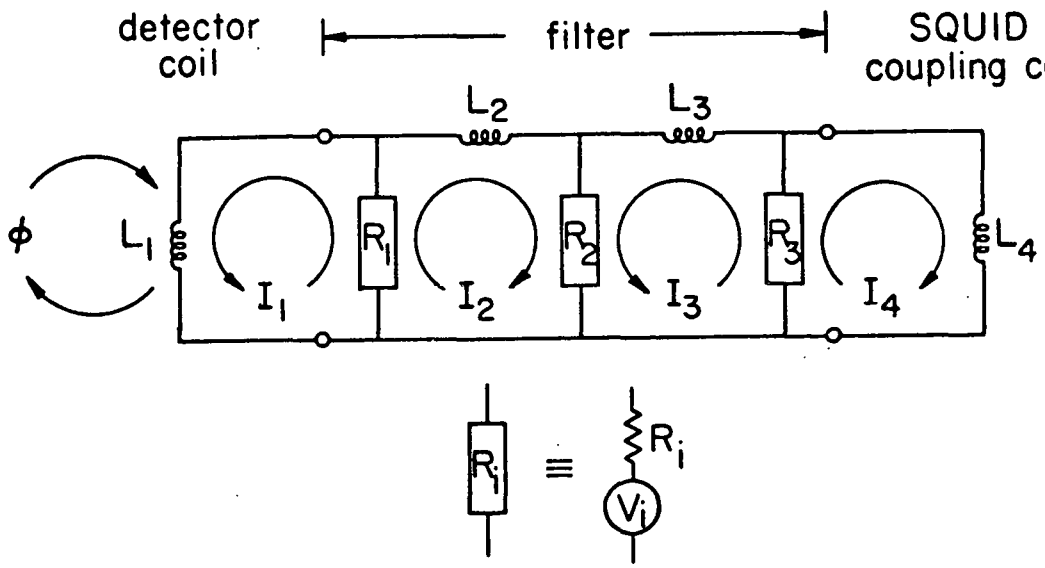

$$\begin{bmatrix} R_1 + i\omega L_i & R_1 & 0 & 0 \\ R_i & R_1 + R_2 + i\omega L_2 & R_2 & 0 \\ 0 & R_2 & R_2 + R_3 + i\omega L_3 & R_3 \\ 0 & 0 & R_3 & R_3 + i\omega L_4 \end{bmatrix} \begin{bmatrix} I_1 \\ I_2 \\ I_3 \\ I_4 \end{bmatrix} = \begin{bmatrix} V_1 - i\omega\phi \\ V_1 - V_2 \\ V_3 - V_2 \\ V_3 \end{bmatrix}$$

$$I_4(\phi) = \frac{\phi}{L_4} \left(\sum_{n=0}^{3} a_n (i\omega)^n \right)^{-1} \quad ; \quad V_i = 0$$

$$a_0 = \frac{L_1 + L_2 + L_3 + L_4}{L_4}$$

$$a_1 = \frac{L_1 + L_2 + L_3}{R_3} + \frac{(L_1 + L_2)(L_3/L_4 + 1)}{R_2} + \frac{(L_2 + L_3 + L_4)L_1/L_4}{R_1}$$

$$a_2 = \frac{(L_1 + L_2)L_3}{R_2R_3} + \frac{(L_2 + L_3)L_1}{R_1R_3} + \frac{(L_3 + L_4)L_1L_2/L_4}{R_1R_2}$$

$$a_3 = \frac{L_1L_2L_3}{R_1R_2R_3} .$$

$$I_4(V_j) = \frac{Vb_j}{L_4} \left(\sum_{n=0}^{3} a_n (i\omega)^n \right)^{-1} \quad ; \quad V_i = (4kTR_iB)^{1/2}$$

$$b_1 = L_1/R_1$$

$$b_2 = \frac{L_1 + L_2}{R_2} + i\omega \frac{L_1L_2}{R_1R_2}$$

$$b_3 = \frac{L_1 + L_2 + L_3}{R_3} + i\omega \left(\frac{L_3(L_1 + L_2)}{R_2R_3} + \frac{L_1(L_2 + L_3)}{R_1R_3} \right) - \omega^2 \frac{L_1L_2L_3}{R_1R_2R_3}$$

Figure 13. a) Low pass filter circuit. L-inductors; R-resistors including Johnson noise, I-currents, ϕ input flux. b) Current I_4 in terms of circuit parameters.

~2μH. Resistors are 0.1 cm of 0.013 cm diam copper wire, ~3μΩ at 4.2 K. Connections from copper wire to niobium wire and niobiuum wire to niobium sheet were spot welded and strain relieved with SC8 epoxy.[78] To ensure superconducting terminal connections, wires and sheet were abraded with emery cloth and cleaned before connection. The wires were then clamped between niobium sheet and a washer made from the sheet material. Performance of the filter was tested and agreement with the predicted frequency response noise level formulae (found in Fig. 13) was obtained. Since installation, the filter has withstood over 50 cycles from 300 K to 4 K without measurable change.

The filter itself is a necessary evil in the SQUID circuit. Although it permits the SQUID to remain locked in feedback mode, by shunting transient signals, it pumps a great deal of Johnson noise directly into the SQUID. It also produces large (> 180°) phase shifts for frequencies $\gtrsim$ 1 Hz which prohibit use of feedback from the SQUID output to a piezoelectric driver in order to null the coil motion. An alternative might be the reduction of the magnetic field strength and/or coupling of the detector coil to the SQUID in effort to reduce high slew rate vibrational noise. The sacrifice in signal amplitude would possibly be offset by the absence of the Johnson noise due to the filter. Because the actual spectrum of vibrational noise was never directly measured (only deconvoluted, using the filter response characteristics) the procedure of removing the filter was not considered worth the risk. Attempts to physically isolate the dilatometer from vibrational noise sources within the cryostat, by using damped spring suspension, failed

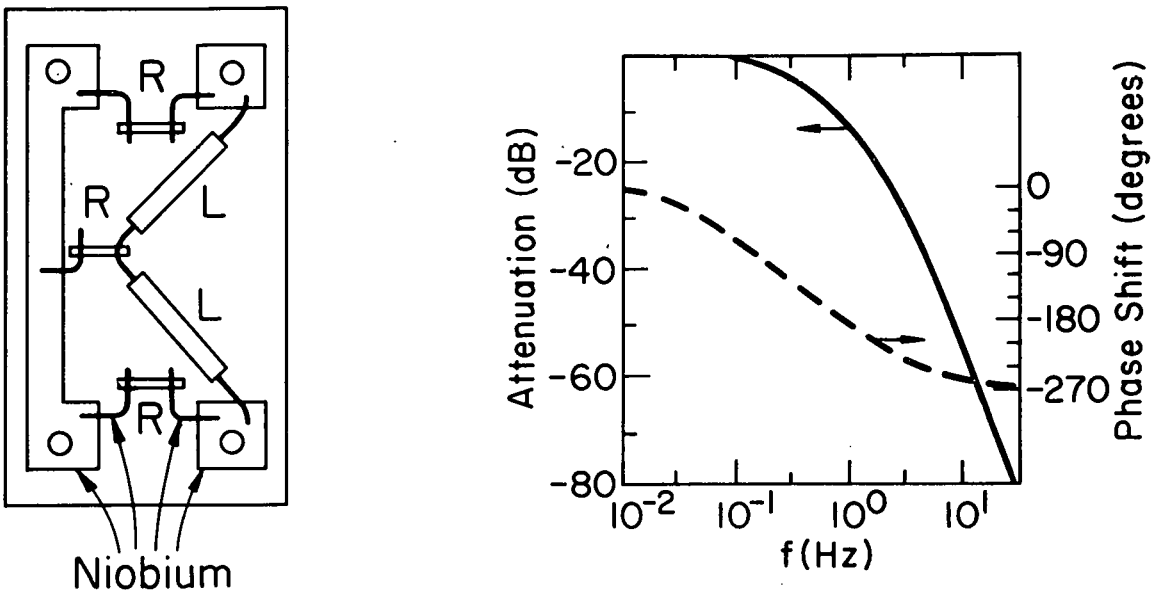

Figure 14a. Layout of low-pass filter (left). R-3μΩ resistors, L-2μH inductors. Attenuation (solid line) and phase shift (dashed line) are plotted as a function of frequency (right).

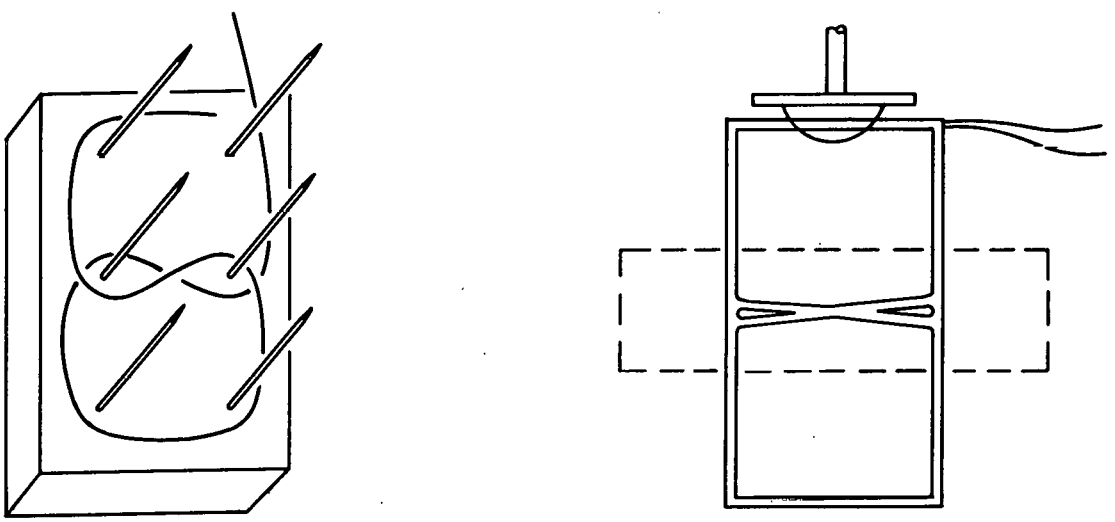

Figure 14b. First turn of figure-8 detector coil on winding form (left). Finished product (right). Also shown are region of B field (within dashed lines) and mounting bracket.

on three counts: poor thermal contact to the refrigerator through the suspension material, production of heat due to internal friction in the springs and oscillation of the whole assembly in the non-uniform B-field of lead shield Pb1 (see Fig. 5). In retrospect, the filter, despite its shortcomings was the proper step given the inevitably high level of environmental vibration.

APPENDIX B

DETECTOR COIL

A brief description of the construction and operation of the detector coil, illustrated in Fig. 14b, will be given. The purpose of the coil was to couple changes of flux, resulting from changes in sample length, into the SQUID circuit.

A figure-8 design was chosen for several reasons. It was experimentally determined that a figure-8 coil produced 60% more EMF/inductance than a simple coil of the same area. The EMF produced by displacement of the figure-8 is effectively doubled by positioning the region of B-field through part of each counter-wound lobe (Fig. 14b), while the increase in inductance per turn in going from a simple to figure-8 design is only 25%. In addition, a figure-8 coil tends to reject externally imposed, spatially uniform B-fields, reducing flux changes from this source by a factor of ~100 over a simple coil. Finally, the straight-line design renders the detector coil less sensitive to pick-up due to vibration in the plane perpendicular to the sample axis (refer to Fig. 5).

The coil consisted of 12 complete turns of 5×10^{-3} cm diam Nb-Ti high-field superconducting wire, insulated with heavy formvar,[83] potted in Stycast 1266 epoxy.[84] Construction entailed winding the wire around 6 steel straight pins protruding through a teflon base (Fig. 14b), applying a sparing amount of epoxy and squeezing the coil flat between the base and a second slab of teflon. The thinner and flatter the coil,

the easier was positioning in the gap of the permanent magnet (shimmed to ~0.15 cm to reduce fringing fields). Once clamped in the form, the coil was baked at 70°C for ~4 hours. Room temperature resistance was tested before and after baking to ensure that no electrical shorts had developed at the cross-over point in the "8". The final product was ≈6μH, designed to match the input impedance of the SQUID plus filter circuits.

Failure of the detector coil to withstand repeated thermal cycling was observed, although visual and electrical inspection never revealed any cause. However, upon failure a noise level in the SQUID circuit was detected at cryogenic temperatures which was typically 10 to 1000 times greater than usual. This occurred in some coils after 20 runs and in others after 3, and could possibly have resulted from a partial or intermittent internal short from one turn to another. Sudden changes of the coil impedance, caused by vibration could account for the noise level observed. Repair required replacement of the coil.

APPENDIX C

THERMAL CIRCUIT

A major obstacle in development of the SQUID dilatometer arose from the presence of spurious signals of thermo-magnetic origin. Noise resulting from a changing temperature (and therefore changing magnetization) of paramagnetic materials in the fringing field of the permanent magnet was comparable in magnitude to thermal expansion signals. For example, a change in detector coil temperature produced an equivalent output of ~0.1 $\mathring{A}$/mK while a change in magnet temperature, or temperature of shield Pb2, produced a response ten times larger. Worst of all was that this noise appeared in synchrony with variations in sample temperature. Therefore, maintaining the entire apparatus at a constant temperature--while heating and cooling the rigidly clamped sample--was crucial to the operation of the dilatometer. A brief description of the method in which heat is shunted in and out of the sample without perturbing the temperature of the dilatometer is given in Chapter III. Additional details about the construction and use of high and low impedance thermal contacts are presented below.

Isolation of the sample from the clamp and frame was accomplished by means of a pair of sapphire-copper-sapphire dry-joint[69] sandwiches on the top and bottom of the sample (see Fig. 5). In Fig. 15, an analogy is drawn between an electrical and thermal circuit, illustrating the current shunting characteristic of the isolation arrangement. Heat current, temperature and thermal impedance ($\dot{Q}$, T and Z) are analogous to

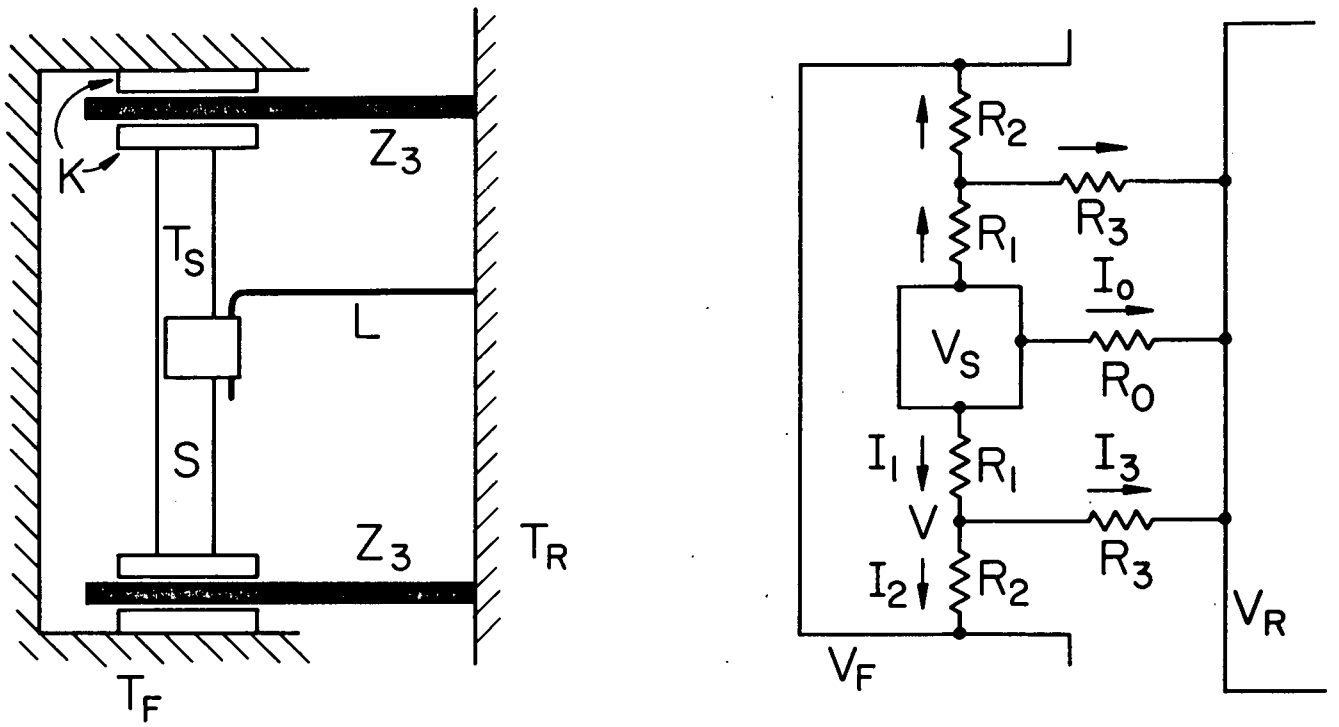

Figure 15. Thermal circuit (left) and electrical circuit analogue (right). S-sample; K-sapphire flats; Z_3-copper shunts; L-heat leak from sample to refrigerator; T_F, T_S, T_R - temperatures of frame, sample, refrigerator (cf. Fig. 5). V-voltage (analogous to T); R-resistance (analogous to Z); I-current(analogous to Q). Heat flowing from sample is shunted away from frame.

electrical current, voltage and resistance (I, V and R) with appropriate subscripts for sample S, frame F and refrigerator R. In particular, R_o represents a heat leak from the sample to the thermal ground, i.e., the refrigerator. In the thermal circuit, R_o was a length of 0.025 cm diam copper wire, bolted at one end to thermal ground and attached at the other to the sample. Contact to dielectric samples was made by welding the wire to a 0.0013 cm copper foil which was, in turn, glued to the sample using GE7031 varnish. This contact provided a minimum thermal impedance as determined by the boundary-resistance limit.[69] R_1 and R_2 represent dry joint inpedances isolating the sample from the frame and R_3 represents the copper shunts to ground from between pairs of R_1 and R_2. For $V_S > V_F > V_R$, $V_R \equiv 0$ and $R_1 = R_2 = \xi R_3$, the current to the frame, $2I_2$ (analogous to heat flow to frame) can be calculated. The change in I_2 with V_S is

$$\frac{\partial I_2}{\partial V_S} = \frac{\partial I_2}{\partial V} \frac{\partial V}{\partial V_2}$$

Since $I_2 = \frac{V - V_F}{R_2}$, $\frac{\partial I_2}{\partial V} = \frac{1}{R_2}$ V_F being regulated at a constant level.

Also $V = \frac{V_S + V_F}{2 + \xi}$ so that $\frac{\partial V}{\partial V_S} \approx \frac{1}{\xi}$, $\xi \gg 2$

Therefore $\frac{\partial I_2}{\partial V_S} = \frac{1}{\xi R_2}$ and $\delta I_2 = \frac{\delta V_S}{\xi R_S}$ C-1

Current I_o is fixed at a level which produces an appropriate value of V_S as well as a constant current load to the refrigerator. Changes in V_S result from variation in point of application of I_o along R_o; the closer to sample S, the higher V_s. (In practice, R_o is divided into two approximately equal parts and I_o is switched, as discussed in Chapter III.) The magnitude of I_o is given by $I_o = \delta V_S / R_o$.

Since $$R_o \approx R_3 \approx R_2/\xi \ ,$$

$$\frac{\delta I_2}{I_o} \approx \frac{1}{\xi^2} \qquad \text{C-2}$$

(It should be noted that in the absence of R_3

$$\delta I_2' = \delta V_S / 2R_2$$

and $$\frac{\delta I_2'}{I_o} = \frac{1}{2\xi} \quad . \quad \text{cf. C-2)} \qquad \text{C-3}$$

The ratio $\delta I_2 / I_o$ is a measure of the variation in (heat) current flowing into the frame relative to the total current being shunted to (thermal) ground. The ratio ξ, of high to low impedance has been measured to be $\sim 10^4$.[69] For typical heat current I_o $\sim$100μW, this implies a maximum variation of heat current to the frame of 10^{-8} I_o $\sim 10^{-12}$W which has been observed to produce no ill-effects. More precisely, by reducing variations of heat flow to the frame and refrigerator, it is possible to electronically regulate T_F and T_R sufficiently well to eliminate thermomagnetic pickup in the SQUID circuit.

APPENDIX D

SAMPLE REFERENCE DATA

Reference data on materials used in this work are tabulated. Under source and specific heat C are listed references only, while data and references are listed under density ρ, longitudinal and transverse sound velocities v_ℓ and v_t and bulk modulus B. An asterisk (under bulk modulus) means that B was calculated under the assumption of isotropy from the v_ℓ and v_t listed, as $B = \rho(v_\ell^2 - \frac{4}{3} v_t^2)$. If more than one entry is listed, it is the first which is used in calculation of the Grüneisen parameter.

Table I. Sample Reference Data

Material	Source	ρ (g/cm^3)	v_ℓ (10^5 cm/sec)	v_t (10^5 cm/sec)	B (10^{11} erg/cm^3)	C
High purity copper	a/	9.03 b/	4.83 b/	2.35 b/	14.2 b/	c/
Spectrosil B	d/	2.20 e/	5.81 e/	3.73 e/	3.6 e/ 3.5 f/ *3.3	e/
Spectrosil WF	d/	2.20 g/	h/	h/	h/	i/
Scotchcast 5	j/	1.14 j/	3.14 j/	1.56 j/	*0.75	j/
Polymethylmethacrylate	k/	1.2	3.18 ℓ/	1.59 ℓ/	0.82 f/ *0.81	f,m/
Arsenic trisulfide	n/	3.2 m,o/	2.91 o/	1.49 o/	*1.8 1.3 p/	m/
Cubic zirconia	q/	5.81 r/	8.08 r/	3.28 r/	*29.6	s/

[a]United Mineral and Chemical Corp., New York, NY.

[b]J. R. Neighbours and C. S. Smith, Acta Metal 2, 591 (1954).

[c]Ref. 72.

[d]Thermal American Fused Quartz Co., Change Bridge Road, Montville, NJ.

Table I. (Continued)

[e]Ref. 15.

[f]Ref. 59.

[g]Ref. 77.

[h]Assumed to be the same as Spectrosil B.

[i]Ref. 80.

[j]Ref. 11.

[k]The PMMA, obtained from stock Plexiglas, was heat treated at 130°C for 2 hours to erase previous thermal history.

[ℓ]K. G. Lyon, USDOE Report IS-T-829-1978 (unpublished).

[m]Ref. 17.

[n]Amorphous As_2S_3 was provided by J. J. Fontenella and was a twin sample to that measured in Ref. 42.

[o]C. Laermans, L. Piché, W. Arnold, S. Hunklinger, in The Physics of Non-Crystalline Solids, ed. by G. H. Frischat (Trans Tech, Aedermannsdorf, Switzerland, 1977), p. 562.

[p]T. N. Claytor and R. J. Sladek, Phys. Rev. B 18, 5842 (1978).

[q]Ceres Corporation, 411 Waverly Oaks Park, Waltham, MA.

[r]Ref. 79.

[s]Ref. 81.

Appendix E

THERMAL EXPANSION DATA

Linear thermal expansion data are tabulated for each of the materials examined. Data are grouped by material and subgrouped in cases in which more than one experimental run was performed. Run designations follow chronological order. Within a listing for a given run, values of linear thermal expansion coefficient $\alpha(T)$ (in units of K^{-1}) follow ascending order in temperature (in units of K). Each datum is accompanied by an experimentally determined uncertainty.

High Purity Copper

Run I

T[K]	$\alpha[K^{-1}]$
0.231	$6.66 \pm 1.66 \times 10^{-11}$
0.281	8.95 ± 1.87
0.281	7.68 ± 1.80
0.330	9.72 ± 3.22
0.380	$1.37 \pm 0.17 \times 10^{-10}$
0.399	1.15 ± 0.11
0.460	1.37 ± 0.16
0.500	1.62 ± 0.31
0.580	1.67 ± 0.26
0.699	1.90 ± 0.29
0.729	1.99 ± 0.28
0.915	2.68 ± 0.21
1.10	3.27 ± 0.27
1.40	4.35 ± 0.44
1.40	4.39 ± 0.64
1.70	5.57 ± 0.18
2.00	6.91 ± 0.34
2.24	8.36 ± 0.78
2.50	$1.01 \pm 0.03 \times 10^{-9}$
2.75	1.30 ± 0.10
3.00	1.47 ± 0.04
3.24	1.83 ± 0.10
3.50	2.13 ± 0.11
3.88	2.55 ± 0.07
4.30	3.39 ± 0.17
4.65	3.93 ± 0.17
5.25	5.46 ± 0.46

Run II

T[K]	$\alpha[K^{-1}]$
0.40	$1.30 \pm 0.16 \times 10^{-10}$
0.58	1.90 ± 0.26
0.70	2.12 ± 0.10
0.77	2.41 ± 0.32
0.85	2.70 ± 0.29
0.93	2.88 ± 0.16
0.93	2.88 ± 0.16
1.00	2.95 ± 0.25
1.20	3.31 ± 0.20
1.20	3.11 ± 0.29
1.40	4.03 ± 0.18
1.40	4.12 ± 0.25
1.70	5.13 ± 0.18
1.79	5.81 ± 0.25
2.40	9.34 ± 0.41
3.20	$1.61 \pm 0.06 \times 10^{-9}$
4.00	2.66 ± 0.05
5.00	4.57 ± 0.90

Run III

T[K]	$\alpha[K^{-1}]$
0.266	$7.89 \pm 1.62 \times 10^{-11}$
0.300	9.98 ± 1.62
0.360	$1.30 \pm 0.26 \times 10^{-10}$
0.400	1.19 ± 0.46
0.440	1.62 ± 0.14
0.480	1.51 ± 0.19
0.530	1.67 ± 0.22
0.530	1.55 ± 0.21
0.580	2.00 ± 0.16
0.640	2.19 ± 0.37
0.700	2.39 ± 0.33
0.770	2.62 ± 0.24
0.850	2.78 ± 0.37
0.850	2.74 ± 0.14
0.930	3.02 ± 0.23
1.00	3.09 ± 0.19
1.20	3.34 ± 0.33
1.20	3.57 ± 0.39
1.40	4.50 ± 0.16
1.70	5.13 ± 0.35
2.00	6.22 ± 0.46
2.40	8.33 ± 0.37
2.80	$1.09 \pm 0.07 \times 10^{-9}$
3.20	1.44 ± 0.03
3.60	1.91 ± 0.05
4.00	2.53 ± 0.09
4.93	4.38 ± 0.02
5.87	7.26 ± 0.04
7.34	$1.35 \pm 0.01 \times 10^{-8}$
8.80	2.16 ± 0.19

Spectrosil B (unirradiated)

Run I

T[K]	$-\alpha[K^{-1}]$
0.255	$2.30 \pm 0.30 \times 10^{-10}$
0.256	1.70 ± 0.31
0.33	2.60 ± 0.70
0.33	2.95 ± 0.33
0.38	3.10 ± 0.30
0.42	3.40 ± 0.27
0.46	4.03 ± 0.27
0.46	4.10 ± 0.27
0.53	4.37 ± 0.60
0.58	5.10 ± 0.50
0.63	5.90 ± 0.60
0.70	6.27 ± 0.54
0.76	7.37 ± 0.47
0.83	8.20 ± 0.40
0.91	8.90 ± 0.47
1.0	$1.022 \pm 0.043 \times 10^{-9}$
1.2	1.35 ± 0.04
1.4	1.63 ± 0.03
1.7	2.23 ± 0.05
2.0	3.19 ± 0.18
2.5	5.12 ± 0.07
3.0	8.08 ± 0.29
3.5	$1.36 \pm 0.03 \times 10^{-8}$
4.3	2.67 ± 0.08
5.0	4.33 ± 0.07
5.5	5.88 ± 0.13
6.0	7.40 ± 0.12
6.6	9.78 ± 0.10
7.2	$1.21 \pm 0.01 \times 10^{-7}$
7.9	1.41 ± 0.01

Neutron Irradiated Spectrosil B

T[K]	$-\alpha[K^{-1}]$
1.00	$7.60 \pm 1.22 \times 10^{-10}$
1.20	9.78 ± 1.04
1.38	$1.27 \pm 0.10 \times 10^{-9}$
1.60	1.60 ± 0.12
1.80	1.83 ± 0.07
2.00	2.23 ± 0.06
2.25	2.78 ± 0.11
2.50	3.34 ± 0.10
2.75	4.19 ± 0.20
3.14	6.25 ± 0.17
3.51	8.78 ± 0.28
4.00	$1.36 \pm 0.06 \times 10^{-8}$
4.50	2.15 ± 0.06
4.50	2.11 ± 0.06
5.00	3.17 ± 0.10
5.50	4.65 ± 0.09
6.00	6.48 ± 0.16
6.00	6.74 ± 0.16
6.60	9.64 ± 0.15
7.16	$1.35 \pm 0.04 \times 10^{-7}$
7.89	1.88 ± 0.04
8.63	2.42 ± 0.06
9.53	3.21 ± 0.02

Spectrosil WF

T[K]	$-\alpha[K^{-1}]$
0.24	$2.83 \pm 0.28 \times 10^{-10}$
0.27	3.04 ± 0.26
0.30	3.43 ± 0.52
0.33	3.32 ± 0.31
0.36	3.72 ± 0.52
0.40	4.48 ± 0.33
0.44	4.65 ± 0.38
0.48	4.79 ± 0.43
0.53	5.35 ± 0.51
0.58	5.90 ± 0.24
0.64	6.57 ± 0.21
0.70	7.29 ± 0.37
0.77	7.80 ± 0.36
0.85	8.61 ± 0.31
0.93	$1.68 \pm 0.08 \times 10^{-9}$
1.00	1.13 ± 0.06
1.10	1.27 ± 0.05
1.20	1.45 ± 0.04
1.40	$1.74 \pm 0.07 \times 10^{-9}$
1.70	2.53 ± 0.17
2.00	3.36 ± 0.14
2.50	5.44 ± 0.19
3.00	9.28 ± 0.16
3.50	$1.48 \pm 0.02 \times 10^{-8}$
4.01	2.43 ± 0.06
4.49	3.75 ± 0.07
5.11	5.94 ± 0.08
5.99	$1.00 \pm 0.02 \times 10^{-7}$

Scotchcast 5

T[K]	$\alpha[K^{-1}]$
0.40	$1.37 \pm 0.18 \times 10^{-10}$
0.48	2.02 ± 0.38
0.53	2.27 ± 0.63
0.58	3.10 ± 0.34
0.64	3.83 ± 0.32
0.70	4.98 ± 0.53
0.70	4.71 ± 0.45
0.77	6.79 ± 0.52
0.85	9.58 ± 0.58
0.93	$1.20 \pm 0.11 \times 10^{-9}$
1.00	1.50 ± 0.08
1.20	2.63 ± 0.06
1.41	4.85 ± 0.15
1.70	9.27 ± 0.23
2.00	$1.76 \pm 0.04 \times 10^{-8}$
2.40	3.35 ± 0.09
2.80	5.62 ± 0.10
3.16	8.42 ± 0.18
4.14	$1.93 \pm 0.04 \times 10^{-7}$
4.45	2.49 ± 0.09
4.73	2.77 ± 0.13
5.65	4.90 ± 0.16
7.24	$1.10 \pm 0.11 \times 10^{-6}$
8.01	1.44 ± 0.15

Polymethylmethacrylate (PMMA)

Run I

T[K]	$\alpha[K^{-1}]$
0.70	$1.63 \pm 0.40 \times 10^{-10}$
0.85	4.62 ± 0.75
1.00	8.99 ± 1.00
1.00	9.25 ± 0.50
1.10	$1.35 \pm 0.18 \times 10^{-9}$
1.20	1.99 ± 0.13
1.40	3.71 ± 0.18
1.70	7.90 ± 0.60
2.01	$1.49 \pm 0.07 \times 10^{-8}$
2.41	3.04 ± 0.05
2.82	5.05 ± 0.25
2.84	5.36 ± 0.03
3.22	8.62 ± 0.19
3.54	$1.39 \pm 0.04 \times 10^{-7}$
3.54	1.35 ± 0.02
3.56	1.38 ± 0.02
4.07	2.05 ± 0.02
4.70	3.71 ± 0.05

Run II

T[K]	$\alpha[K^{-1}]$
0.58	$5.49 \pm 1.01 \times 10^{-11}$
0.64	9.84 ± 1.97
0.70	$1.50 \pm 0.21 \times 10^{-10}$
0.77	2.48 ± 0.38
0.85	4.22 ± 0.49
0.93	6.03 ± 0.52
1.00	8.10 ± 0.75
2.00	$1.48 \pm 0.04 \times 10^{-8}$
4.05	$1.87 \pm 0.04 \times 10^{-7}$

As_2S_3

Run I

T[K]	$\alpha[K^{-1}]$
0.48	$8.01 \pm 1.90 \times 10^{-11}$
0.53	$1.07 \pm 0.16 \times 10^{-10}$
0.58	1.49 ± 0.14
0.64	1.97 ± 0.20
0.70	2.78 ± 0.20
0.77	3.73 ± 0.28
0.85	4.87 ± 0.33
0.85	5.06 ± 0.52
0.93	6.58 ± 0.38
1.00	8.50 ± 0.55
1.10	$1.21 \pm 0.07 \times 10^{-9}$
1.20	1.72 ± 0.05
1.23	1.70 ± 0.09
1.40	3.07 ± 0.18
1.47	3.24 ± 0.15
1.80	6.50 ± 0.25
2.00	9.34 ± 0.23
2.15	$1.17 \pm 0.03 \times 10^{-8}$
2.40	1.85 ± 0.04
2.80	3.32 ± 0.08
3.22	5.35 ± 0.15
3.59	7.96 ± 0.20
3.99	$1.21 \pm 0.04 \times 10^{-7}$
4.39	1.69 ± 0.04

Run II

T[K]	$\alpha[K^{-1}]$
0.58	$1.36 \pm 0.29 \times 10^{-10}$
0.64	1.75 ± 0.17
0.70	2.90 ± 0.29
0.85	4.94 ± 0.33
1.00	8.51 ± 0.27
2.00	9.10 ± 0.23
2.40	$1.78 \pm 0.04 \times 10^{-8}$
3.20	5.14 ± 0.07
4.00	$1.18 \pm 0.01 \times 10^{-7}$
4.00	1.15 ± 0.01
5.56	3.58 ± 0.03
7.12	7.82 ± 0.13

$ZrO_2:Y_2O_3$ (16%)

T[K]	$\alpha[K^{-1}]$
0.70	$7.24 \pm 1.21 \times 10^{-11}$
0.77	6.81 ± 0.97
0.85	7.23 ± 1.05
0.93	$1.00 \pm 0.10 \times 10^{-10}$
1.00	1.11 ± 0.13
1.00	1.00 ± 0.15
1.20	1.32 ± 0.11
1.40	1.48 ± 0.09
1.70	2.00 ± 0.02
2.00	2.21 ± 0.13
2.40	3.08 ± 0.16
2.80	3.79 ± 0.15
3.20	4.90 ± 0.20
4.00	7.58 ± 0.22
5.00	$1.21 \pm 0.10 \times 10^{-9}$
6.00	1.71 ± 0.08

APPENDIX F

EFFECTS OF DENSITY OF STATES AND SPATIAL AVERAGING

In Chapter V, consideration was given to the value of $D = D_{avg}$, inferred by thermal expansion measurements, relative to $D = D_{rms}$, derived from relaxation attenuation experiments. In particular, a distribution in D (Eq. V-3) was invoked to explain the reason that $D \approx 1eV$, taken from ultrasonic measurements, was inappropriately large in the calculation of Γ, the Grüneisen parameter. Alternate strategies for explaining the apparently reduced value of deformation potential D might entail averaging over the proposed energy density of states in ε and Δ (Eq. II-2), or detailed spatial averaging. It is argued below, that neither of these ploys can reconcile large values of deformation potential and small Grüneisen parameters.

The Grüneisen parameter Γ_i for the i-th TLS is given by Eq. II-11 as

$$\Gamma_i = \frac{1}{E_i}\left(\frac{\varepsilon}{E}\frac{\partial \varepsilon}{\partial e} + \frac{\Delta}{E}\frac{\partial \Delta}{\partial e}\right)_i$$

$$\Gamma_i = \left(\frac{\varepsilon}{E}\right)^2 \Gamma_\varepsilon + \left(\frac{\Delta}{E}\right)^2 \Gamma_\Delta \qquad \text{F-1}$$

in which $\Gamma_x = \frac{\partial \ell n x}{\partial e}$.

Γ, averaged over all TLS can be calculated as an average over ε and Δ.

$$\langle\Gamma\rangle = \int d\varepsilon \int d\Delta \; n(\varepsilon,\Delta) \; \Gamma(\varepsilon,\Delta)$$

using the expression in F-1 as $\Gamma(\varepsilon,\Delta)$. Assuming Γ_ε and Γ_Δ to be constant, i.e., no distributions in deformation potentials,

$$\langle\Gamma\rangle = \langle\frac{\varepsilon^2}{E^2}\rangle\Gamma_\varepsilon + \langle\frac{\Delta^2}{E^2}\rangle\Gamma_\Delta \quad . \qquad \text{F-2}$$

The averages appearing in angular brackets in F-2 can be calculated as functions of energy E, using the density of states $n(\varepsilon,\Delta)$ suggested in Ref. 21, and appear plotted in Fig. 16. In the energy range of interest, 0.1 K $\lesssim$ E/k $\lesssim$ 1 K, $\langle\varepsilon^2/E^2\rangle \to 1$ while $\langle\Delta^2/E^2\rangle \to 0$ with increasing E. Therefore,

$$\langle\Gamma\rangle \approx \langle\frac{\varepsilon^2}{E^2}\rangle\Gamma_\varepsilon \approx \Gamma_\varepsilon \quad .$$

No reduction in $\langle\Gamma\rangle$ is obtained through this averaging process since $\Gamma_\varepsilon \approx D/E \approx 1eV/E \gtrsim 10^4$ for all TLS having E/k $\lesssim$ 1 K.

Another group of arguments involve the spatial relationship of TLS and phonons. If the coupling of thermal phonons to TLS through the tensor deformation potential $D_{\alpha\beta}$ were highly anisotropic, it might be that only phonons of energy E with select wavevectors and polarization could modulate the TLS energy. Under this condition, an adiabatic compression experiment as in Ref. 60 would measure a reduced value of Γ since uniaxial stress would alter the energy of only those TLS which

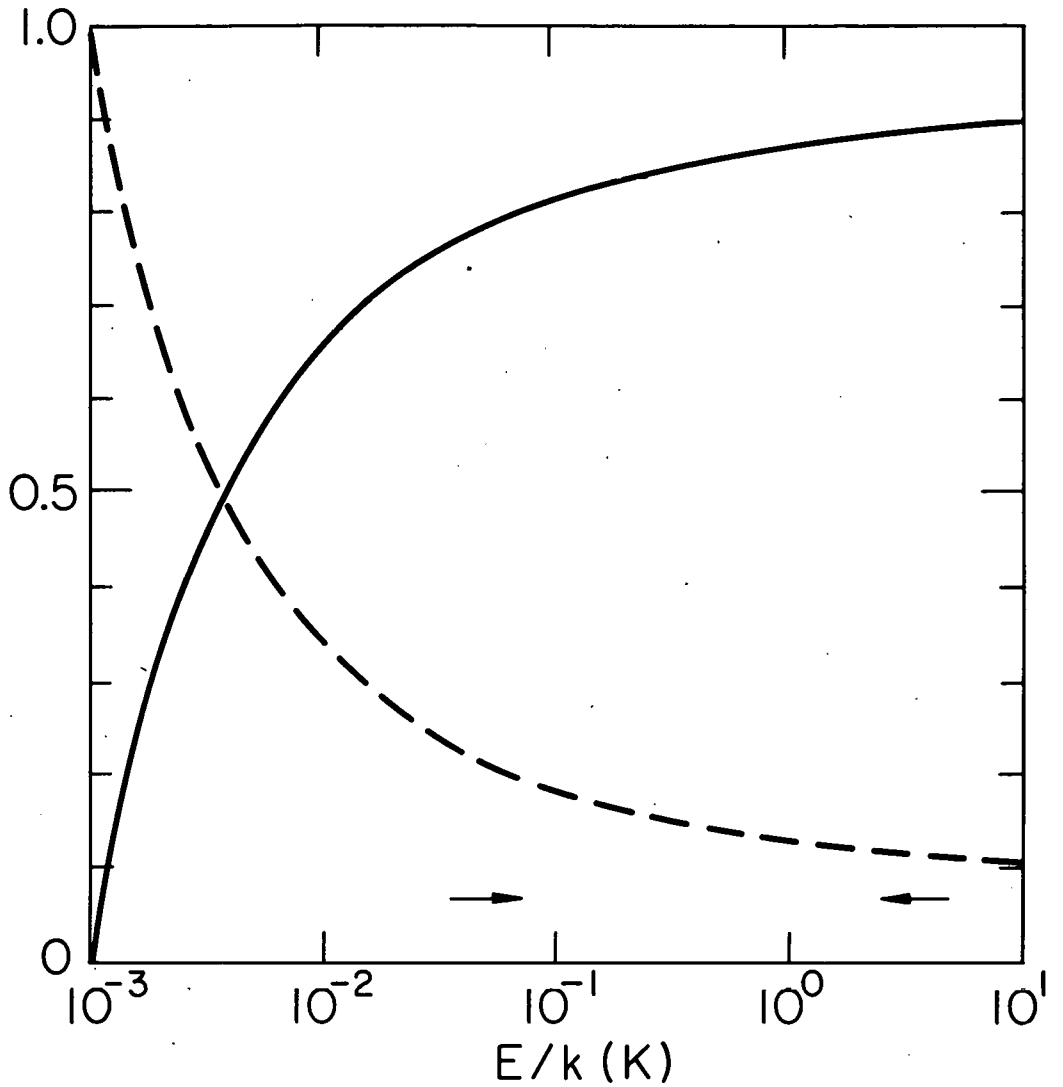

Figure 16. Using the density of states suggested in Ref. 21, average values of $\langle\Delta^2/E^2\rangle = (E^2 - \Delta_{min}^2)^{1/2} E^{-1}(\ell n((E + (E^2 - \Delta_{min}^2)^{1/2}) / \Delta_{min}))^{-1}$ (dashed line) and $\langle\varepsilon^2 / E^2\rangle = 1 - \langle\Delta^2 / E^2\rangle$ (solid line) are plotted. Using $\Delta_{min} = 10^{-7}$ eV ($\approx 10^{-3}$ K) as the minimum value of overlap (corresponding to a relaxation time[38] (Eq. II-8) $\tau \approx \tau_{exp} \approx 1$ sec), it is apparent that $\langle\varepsilon^2 / E^2\rangle$ dominates at $E/k > 0.1$ K. Arrows indicate approximate range of energies probed by present thermal expansion measurements.

could couple to the imposed strain. However, the value of inferred from relaxation attenuation measurements would also reflect the angular and polarization-dependent coupling. In short, the reduction of $\beta(T)$ or Γ and that of D due to anisotropic coupling should be very similar, lending no explanation for a small thermal expansion in the face of a measured value of $D \approx 1eV$. Furthermore, it should be noted that the coupling constants of TLS to transverse and to longitudinal phonons are similar in magnitude.[38]

On the other hand, a TLS might change configuration upon excitation in a very anisotropic manner. For example, a spherical defect may expand along one axis only. Indeed, anisotropic thermal expansion is observed in crystals.[35] Conceivably, $\partial E/\partial \ell nV$ for the excitation could be $\approx$ 1eV while $\partial \ell$ in two orthogonal directions could be small (or even negative). The effect would be expected to reduce $\beta(T)$ by a factor of $\sim \frac{1}{3}$ from that predicted by ultrasonic measurement of D. This factor does not suffice to explain, for example, a $\Gamma \approx 1$ for SC5 for which $D \approx 1eV$[11] would imply[39] $\Gamma \sim 10^4$.

Along the same line of reasoning, it has been suggested[55] that a TLS could change configurations upon excitation with no attendant change in volume. (Calculation of thermal conductivity and specific heat are not affected by this assumption.) However, only phonons with wavelength roughly that of the defect size could couple to such a TLS. In the use of very long wavelengths in Ref. 60 (essentially a static measurement on the scale of 1 K phonons), as well as in ultrasonic experiments,[54] coupling of TLS to long wavelength phonons is observed.

It can therefore be concluded that neither averaging of energy nor spatial coordinates can account for small Γ and large D_{rms}. It was for this reason that the distribution in D was adopted.

REFERENCES

1. For a review, see Amorphous Solids: Low-Temperature Properties, ed. by W. A. Phillips (Springer Verlag, Berlin, 1981).

2. R. C. Zeller, M.S. Thesis (Cornell University, 1974) (unpublished). R. B. Stephens, Ph.D. Thesis (Cornell University, 1974) (unpublished).

3. M. P. Zaitlin and A. C. Anderson, Phys. Rev. Lett. 33, 1158 (1974).

4. M. P. Zaitlin, L. M. Scherr and A. C. Anderson, Phys. Rev. B 12, 4487 (1975)

5. G. L. Salinger, in Amorphous Materials, ed. by R. W. Douglas and B. Ellis (Wiley, New York, 1970), p. 475.

6. A. C. Anderson, W. Reese and J. C. Wheatley, Rev. Sci. Instrum. 34, 1386 (1963).

7. G. S. Cieloszyk, M. T. Cruz and G. L. Salinger, Cryogenics 13, 718 (1973).

8. R. B. Stephens, Phys. Rev. B 8, 2896 (1973).

9. G. K. White, S. B. Woods and M. T. Elford, Phys. Rev. 112, 111 (1958).

10. J. E. Graener, B. Golding, R. J. Schutz, F.S.L. Hsu and H. S. Chen, Phys. Rev. Lett. 39, 1480 (1977).

11. D. S. Matsumoto, C. L. Reynolds and A. C. Anderson, Phys. Rev. B 19, 4277 (1979).

12. M. Wun and N. E. Phillips, Cryogenics 15, 36 (1975).

13. J. C. Lasjaunias, D. Thoulouze and F. Pernot, Solid State Commun. 14, 957 (1974).

14. J. C. Lasjaunias, A. Ravex, M. Vandorpe and S. Hunklinger, Solid State Commun. 17, 1045 (1975). In addition, thermal conductivity was found to be independent of OH^- concentrations.

15. T. L. Smith, P. J. Anthony and A. C. Anderson, Phys. Rev. B 17, 4997 (1978).

16. R. C. Zeller and R. O. Pohl, Phys. Rev. B 4, 2029 (1971).

17. R. B. Stephens, Phys. Rev. B 13, 852 (1976).

18. P. Flubacher, A. J. Leadbetter, J. A. Morrison and B. P. Stoicheff, J. Phys. Chem. Solids 12, 53 (1959).

19. N. Bilir and W. A. Phillips, Philos. Mag. 32, 113 (1975).

20. P. W. Anderson, B. I. Halperin and C. M. Varma, Philos Mag. 25, 1 (1971).

21. W. A. Phillips, J. Low Temp. Phys. 7, 351 (1972).

22. H. B. Rosenstock, J. Phys. Chem. Solids 23, 659 (1962).

23. P. Fulde and H. Wagner, Phys. Rev. Lett. 27, 1280 (1971).

24. S. Takeno and M. Goda, Prog. Theor. Phys. 48, 1468 (1972).

25. J. Jäckle, L. Piché, W. Arnold and S. Hunklinger, J. Non-Cryst. Solids 20, 365 (1976).

26. K. K. Mon and N. W. Ashcroft, Solid State Commun. 27, 609 (1978).

27. A. S. Wagh, J. Phys. Chem. Solids 42, 185 (1981).

28. J. C. Phillips, Phys. Rev. B 24, 1744 (1981).

29. P. J. Anthony and A. C. Anderson, Phys. Rev. B 16, 3827 (1977).

30. J. W. Gardner and A. C. Anderson, Phys. Rev. B 23, 474 (1981).

31. D. A. Ackerman, D. Moy, R. C. Potter, A. C. Anderson and W. N. Lawless, Phys. Rev. B 23, 3886 (1981).

32. E. Bonjour, R. Calemczuk, R. Lagnier and B. Salce, J. Phys. (Paris) 42, C6 (1981).

33. G. K. White, Phys. Rev. Lett. 34, 204 (1975).

34. D. A. Ackerman and A. C. Anderson, Phys. Rev. Lett. (submitted).

35. For a review, see T.H.K. Barron, J. G. Collins and G. K. White, Adv. Phys. 29, 609 (1980).

36. E. Grüneisen, Ann. Phys. 39, 257 (1912).

37. See Ref. 1, Chapter 4.

38. For a review, see S. Hunklinger and W. Arnold, in Physical Acoustics, ed. by W. P. Mason and R. N. Thurston (Academic Press, New York, 1976), Vol. 12, p. 155.

39. W. A. Phillips, J. Low Temp. Phys. 11, 757 (1973).

40. C. R. Case, K. O. McLean, C. A. Swenson and G. K. White, A.I.P. Conf. Proc. 3, 183 (1972); C. R. Case and C. A. Swenson, Phys. Rev. B 9, 4506 (1974).

41. D. A. Ackerman and A. C. Anderson, Rev. Sci. Instrum. (to be published).

42. G. J. Morgan, G. K. White and J. G. Collins, Philos. Mag. B 43, 1039 (1980).

43. R. O. Pohl and G. L. Salinger, Ann. N.Y. Acad. Sci. 279, 150 (1976).

44. D. F. Gibbons, J. Phys. Chem. Solids 11, 246 (1959).

45. O. L. Anderson and G. J. Dienes, in Non-Crystalline Solids, ed. by G. Frechette (Wiley, New York, 1960), p. 449.

46. J. T. Krause and C. R. Kurkjian, J. Am. Ceram. Soc. 51, 226 (1968).

47. G. K. White, J. A. Birch and M. H. Manghnani, J. Non-Cryst. Solids 23, 99 (1977).

48. G. K. White and J. A. Birch, Phys. Chem. Glasses 6, 85 (1965).

49. G. K. White, Cryogenics 4, 2 (1964).

50. M. Blackman, Philos. Mag. 3, 831 (1958).

51. A. E. Clark and R. E. Strakna, Phys. Chem. Glasses 3, 121 (1962).

52. F. Reif, Fundamentals of Statistical and Thermal Physics (McGraw-Hill Book Co., New York, 1965), p. 416.

53. M. P. Zaitlin and A. C. Anderson, Phys. Rev. B 12, 4475 (1975).

54. B. Golding and J. E. Graebner, Phys. Rev. Lett. 37, 852 (1976); J. E. Graebner and B. Golding, Phys. Rev. B 19, 964 (1979); J. L. Black and B. I. Halperin, Phys. Rev. B 16, 2879 (1977); J. Jäckle, Z. Phys. 257, 212 (1972); see Ref. 1, Chapter 7.

55. M. W. Klein, B. Fischer, A. C. Anderson and P. J. Anthony, Phys. Rev. B 18, 5887 (1978).

56. J. A. Sussmann, Phys. Kondens. Mater. 2, 146 (1964).

57. J. L. Black, Phys. Rev. B 17, 2740 (1978).

58. B. Fischer and M. W. Klein, Solid State Commun. 35, 37 (1980).

59. K. G. Lyon, G. L. Salinger and C. A. Swenson, Phys. Rev. B 19, 4231 (1979).

60. O. B. Wright and W. A. Phillips, Physica (Utr.) 108B, 859 (1981).

61. M. Popoular, J. Phys. C. 5, 1943 (1972).

62. M. W. Klein, Private communication.

63. For a review of SQUID theory and application, see O. V. Lounasmaa, Experimental Principles and Methods Below 1 K (Academic Press, London, 1974), Chapter 7.

64. S.H.E. Corp., 4174 Sorrento Valley Boulevard, San Diego, CA 92121.

65. K. G. Lyon, G. L. Salinger, C. A. Swenson and G. K. White, J. Appl. Phys. 48, 865 (1977).

66. G. M. Graham and F.N.D. Pereira, J. Appl. Phys. 42, 3011 (1970).

67. V. M. Pudalov and M. S. Khaikin, Cryogenics 9, 128 (1969). These authors found the output of a quartz transducer to vary by factors of 1.5 to 2 between cryogenic runs.

68. A. C. Anderson, Rev. Sci. Instrum. 51, 1603 (1980).

69. D. A. Ackerman and A. C. Anderson, Rev. Sci. Instrum. 53, 100 (1982).

70. R. J. Soulen, J. Phys. (Paris) 39, C6-1166 (1978); J. F. Schooley, J. Phys. (Paris) 39, C6-119 (1978); R. J. Soulen, Cryogenics 14, 250 (1974); J. F. Schooley, G. A. Evans and R. J. Soulen, Cyrogenics 20, 193 (1980).

71. A. C. Anderson, R. E. Peterson and J. E. Robichaux, Rev. Sci. Instrum. 41, 528 (1970).

72. E. J. Cotts and A. C. Anderson, J. Low Temp. Phys. 43, 437 (1981). The present expansion measurements were obtained on the EPT76 temperature scale, while the specific heat data were obtained on the T_{62} vapor pressure scale.

73. F. R. Kroeger and C. A. Swenson, J. Appl. Phys. 48, 853 (1977); and papers cited therein.

74. The calibration was consistent with that computed from the circuit parameters as discussed in Chapter III.

75. K. O. McLean, C. A. Swenson and C. R. Case, J. Low Temp. Phys. 1, 77 (1972).

76. J. G. Collins, Ann. Acad. Sci. Fennicae A. VI 210, 239 (1966).

77. S. H. Mahle and R. D. McCammon, Phys. Chem. Glasses 10, 222 (1969). The hydroxyl concentration of Spectrosil WF, Infrasil, Vitreosil OG and Spectrosil B are determined to be 20, 30, 430 and 1190 ppm, respectively.

78. Manufactured by 3M Co., St. Paul, MN 55101.

79. I. L. Chistyi, I. L. Fabelinskii, V. F. Kitaeva, V. V. Osiko, Yu. V. Pisarevskii, I. M. Sil'vestrova and N. N. Sobolev, J. Raman Spectroscopy 6, 183 (1977).

80. W. M. MacDonald and A. C. Anderson (unpublished).

81. F. J. Walker and A. C. Anderson (unpublished).

82. Use of a distribution was suggested by the analysis used in Ref. 39.

83. Manufactured by Supercon Inc., 9 Erie Drive, Natick, MA 01760.

84. Manufactured by Emerson and Cuming, Inc., 3450 Commercial, Northbrook, IL 60062.

VITA

David A. Ackerman was born in [redacted].

He attended public school in New Jersey and graduated from Livingston High School in 1972. He then entered Cornell University, Ithaca, New York and received the Bachelor of Arts degree in 1976. Since then, he has attended the University of Illinois in Urbana-Champaign, Illinois, from which he received the Master of Science degree in Physics in 1978. He was awarded a University Fellowship by the University of Illinois in 1979 and a Research Fellowship from the General Electric Foundation in 1980.